

Report

R-15-11

May 2015



Further metallographic analysis of MiniCan SCC test specimens

Suzanne Aggarwal
Venugopal Addepalli
Nicholas Smart

SVENSK KÄRNBRÄNSLEHANTERING AB

SWEDISH NUCLEAR FUEL
AND WASTE MANAGEMENT CO

Box 250, SE-101 24 Stockholm
Phone +46 8 459 84 00
skb.se

SVENSK KÄRNBRÄNSLEHANTERING

ISSN 1402-3091

SKB R-15-11

ID 1473080

May 2015

Further metallographic analysis of MiniCan SCC test specimens

Suzanne Aggarwal, Venugopal Addepalli, Nicholas Smart
Amec Foster Wheeler

This report concerns a study which was conducted for Svensk Kärnbränslehantering AB (SKB). The conclusions and viewpoints presented in the report are those of the authors. SKB may draw modified conclusions, based on additional literature sources and/or expert opinions.

A pdf version of this document can be downloaded from www.skb.se.

© 2015 Svensk Kärnbränslehantering AB

Summary

This report has been prepared in response to further requests for metallurgical investigation of some aspects of a project carried out for SKB on the WOL and U-bend specimens that were removed from the MiniCan experiment in 2011, following on from previous metallurgical analysis on the specimens in 2013. The specimens were broken out from existing metallurgical Bakelite mounts and examined using scanning electron microscopy and optical microscopy to evaluate the extent of any localised corrosion.

The two types of specimens reviewed were WOLs (wedge opened loaded) and U-bend specimens. The material is an oxygen-free phosphorous-doped copper alloy. There are two WOLs, WOL A and WOL B, and three U-bends, 94UG, 95UG and untested.

The requirements of this work were to determine:

- Whether any crack growth that could be attributed to stress corrosion cracking (SCC) had occurred from the pre-crack in the WOL specimens
- Whether any pitting had occurred on the U-bend specimens in either the unstressed or stressed regions of the samples.

There was no evidence of crack growth that could be attributed to SCC on the WOL fracture faces. However there was evidence of pitting on one of the U-bend specimens and general corrosion on the second U-bend specimen.

The WOL pre-crack fracture faces had an oxygen-rich deposit, whilst the pits on the U-bend also showed evidence of a deposit with the same chemical composition. There was also evidence of calcium on the specimens' surfaces, which suggests that the deposit may have occurred during post-test wet storage in groundwater.

Sammanfattning

I denna rapport redovisas en fortsatt metallografisk utvärdering av kopparprover från SKB:s försöks-serie Minican. De undersökta proverna återtog från Äspölaboratoriet 2011 och en första omgång metallografiska analyser genomfördes och rapporterades 2013. Dessa prover har nu brutits ur den bakelit i vilken de varit monterade och undersökts med svepelektronmikroskopi och optisk mikroskopi. Undersökningen har gjorts i syfte att utvärdera omfattningen av lokala korrosionsangrepp.

Kopparprover av två typer har undersökts; förspräckta så kallade WOL-prover (wedge open loaded), samt U-böjda prover (U-bend). Båda provtyperna är tillverkade av SKB:s kapselkoppar, en syrefri fosfordopad kopparlegering. Undersökningen omfattar två förspräckta prover (WOL A och WOL B) och tre U-böjda prover (94UG, 95UG och ”untested”).

Arbetet syftar till att besvara följande två frågor:

- Huruvida spricktillväxt skett i de förspräckta proverna (WOL) och om denna spricktillväxt i så fall kan härledas till spänningskorrosion
- Huruvida lokaliserad korrosion skett på flata eller böjda delar av ytan hos böjda prover (U-bends)

Ingen spricktillväxt som kan härledas till spänningskorrosion har kunnat identifieras på de förspräckta proverna. Däremot fanns tecken på lokal korrosion på ett av de böjda proverna, medan det andra av de exponerade böjda proverna endast bar spår av allmän korrosion.

De sprickytor i de förspräckta proverna som varit exponerade under försökets gång hade en syrehaltig beläggning. Syre återfanns även i de lokala korrosionsangrepp som identifierats på ett av de böjda proverna. Även kalcium återfanns på de analyserade provytorna, vilket tyder på att beläggningen kan ha bildats under förvaring av proverna i grundvatten efter att experimentet på Äspölaboratoriet avbrutits.

Contents

| | | |
|----------|---|-----------|
| 1 | Technical overview and outline of work | 7 |
| 1.1 | Introduction | 7 |
| 1.2 | Scope of Work | 7 |
| 1.2.1 | WOL specimens | 7 |
| 1.2.2 | U-bend specimens | 8 |
| 2 | Methodology | 9 |
| 3 | Results | 11 |
| 3.1 | WOL specimens | 11 |
| 3.1.1 | Photographic images of mounted WOL specimens | 11 |
| 3.1.2 | Confocal microscope images, visual features and average crack length of WOL fracture faces | 12 |
| 3.1.3 | SEM (Scanning electron microscope) images of WOL fracture faces | 14 |
| 3.1.4 | Conclusions from examination of WOL specimens | 19 |
| 3.2 | U-bend specimens | 19 |
| 3.2.1 | Photographic images of U bend specimens | 19 |
| 3.2.2 | Confocal microscope images, surface roughness (Ra) and visual features of U-bend outer surfaces | 21 |
| 3.2.3 | SEM microscope images and EDX (energy dispersive spectroscopy) analysis of U-bend surfaces | 26 |
| 4 | Overall Conclusions | 33 |
| | References | 35 |
| | Appendix A | 37 |

1 Technical overview and outline of work

1.1 Introduction

A series of in situ corrosion experiments, known as MiniCan, have been operating in SKB's Äspö underground research laboratory since 2007. In 2011, one of the five modules in the MiniCan project (Experiment 3) was removed and analysed by Amec Foster Wheeler (Smart et al. 2012). Figure 1-1 illustrates the design of MiniCan Experiment 3 as it was mounted in the borehole. Subsequently, metallographic analysis was carried out on the SCC (stress corrosion cracking) test specimens mounted in the borehole of Experiment 3, namely two WOL (wedge open loaded) specimens and two U-bend samples. Results from this analysis were published in Smart et al. (2013).

Due to slightly different appearances of the crack fronts of the two WOL specimens, and the observation of a few indentations on one U-bend, further metallographic analyses were conducted in order to establish whether:

- Any crack growth that could be attributed to SCC had occurred from the pre-crack in the WOL specimens (WOLs).
- Whether any pitting had occurred on the U-bend specimens (U-bends) in either the unstressed or stressed regions of the samples.

1.2 Scope of Work

1.2.1 WOL specimens

The two pre-cracked WOL specimens were embedded in Bakelite, as they were mounted and polished for previous metallurgical analysis (Smart et al. 2013). Consequently, removal of the specimens from the Bakelite for analysis was required. Fatigue crack opening of the WOL specimens to expose the fracture faces was also required. Fracture face analysis of the WOLs was carried out for this report to support previous metallurgical investigations.

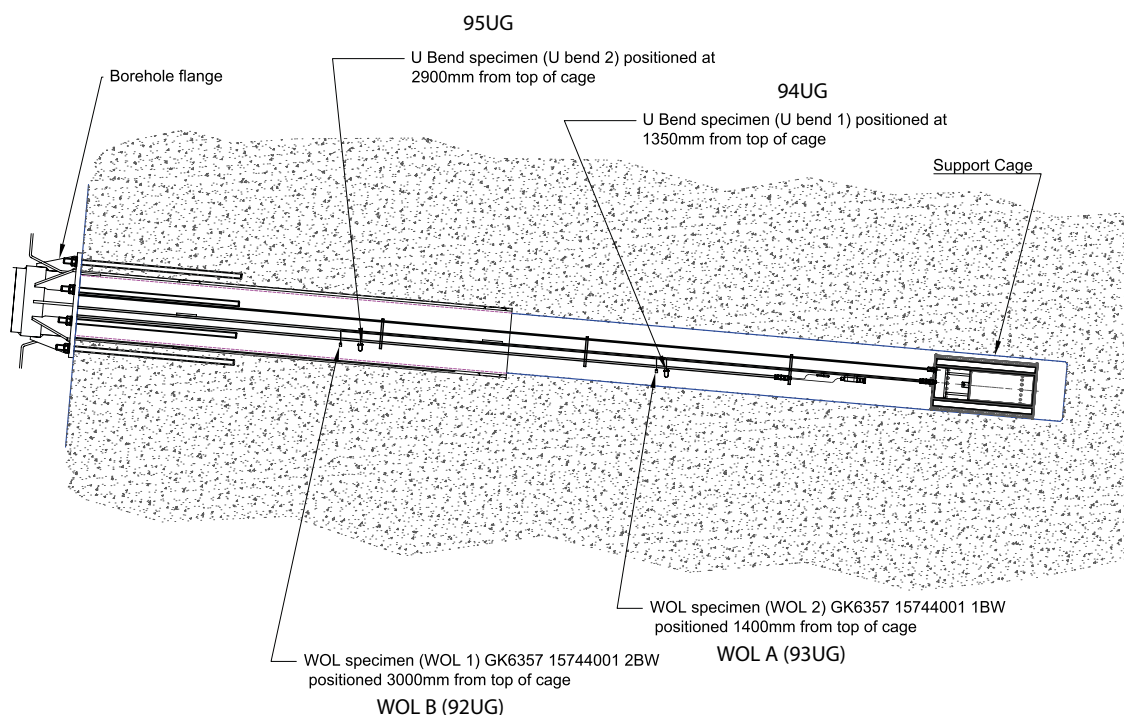


Figure 1-1. Schematic of MiniCan test with mount codes (UG) from previous metallographic investigation (Smart et al. 2013).

1.2.2 U-bend specimens

Sections of the curved part of the U-bend samples were also embedded in Bakelite, as they were previously mounted and polished in cross-section for an earlier metallurgical report (Smart et al. 2013), in order to establish whether any SCC or pitting had occurred. Each U-bend had been previously sectioned into three pieces across the U-bend position and the flat parts of the U-bends (where the bolts were threaded through) had been removed.

Figure 1-2 shows the section lines for each U-bend and the terminology used to describe the different specimens. Two out of three sections per U-bend were mounted in Bakelite for previous metallurgical analysis (Smart et al. 2013). The previously mounted sections exhibited small shallow pit-like depressions on the surface, which were previously attributed to strain-induced features (Smart et al. 2013).

The aim of the work presented in the current document was to examine the surfaces of the curved part (stressed) and flat (unstressed) regions of the U-bends to establish the morphology of any depressions and to conclude whether they were due to pitting corrosion or whether they were strain-induced features. Both the unmounted and mounted sections were analysed as well as an untested U-bend, which had not been exposed to the deep groundwater at Äspö. The untested U-bend was created from copper strip and formed into the same curvature as the tested U-bends, using the same techniques.

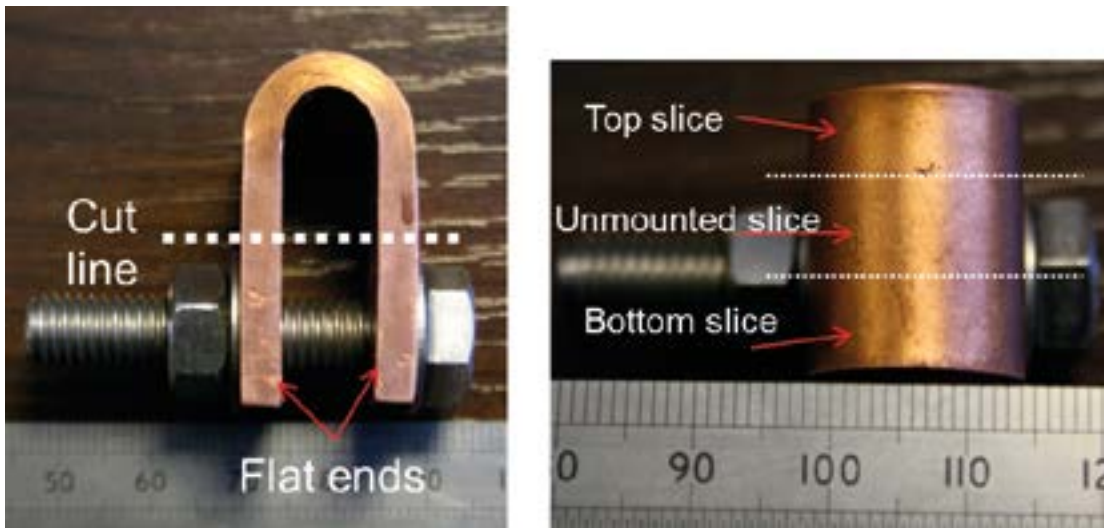


Figure 1-2. Sectioning of U-bend specimens.

2 Methodology

- The first task was to photograph all pieces for this investigation. All sections (mounted and unmounted) were photographed at this stage. A log of all specimens and sections that were included in this analysis is given in Table 2-1.
- The second task was to remove the WOLs and U-bend sections from any Bakelite mounts for metallurgical investigation.
- The third task was for the previously pre-cracked WOLs to be pulled open to examine the fracture faces, to determine whether there were any effects from SCC. This examination was carried out using optical macroscopy, Alicona confocal microscope imaging and SEM (scanning electron microscope) imaging of each fracture face.
- The fourth task was the investigation of the surface features of the stressed (U-bend) and unstressed (unbent section of the U-bends).

Figure 1-2 identifies sections of the U-bends. The surface investigation was carried out using optical macroscopy, Alicona confocal microscope imaging and SEM investigation of the surface features of sections of the U-bends.

Table 2-1. Specimens and specimen sections analysed.

| MiniCan specimen ID | Position | Amec Foster Wheeler Specimen ID | Amec Foster Wheeler Section IDs | Bakelite Mount code |
|-------------------------------------|---------------------------|---------------------------------|--|---------------------|
| WOL 1 GK6357 15744001 2BW | Close to bore-hole flange | WOL B | WOL B1 & WOL B2 | 92UG |
| WOL 2 GK6357 1574401 1BW | Close to cage | WOL A | WOL A1 & WOL A2 | 93UG |
| U bend 1 (1350 mm from top of cage) | Close to cage | U-bend | Top slice, bottom slice, unmounted slice | 94UG |
| U bend 2 (2900 mm from top of cage) | Close to bore-hole flange | U-bend | Top slice, bottom slice, unmounted slice | 95UG |

3 Results

3.1 WOL specimens

3.1.1 Photographic images of mounted WOL specimens

Figure 3-1 shows the WOL specimens before they were removed from the Bakelite mounts and Figure 3-2 shows the opened WOL specimens; there was a range of discoloration on the notch and pre-crack area, along with fresh shiny surfaces on the fast fracture areas. The pre-crack region is evident from the thumbnail shapes emanating from the notch created in the WOLs. WOL B sections appear to have a much darker deposit on the surface of the pre-crack region.

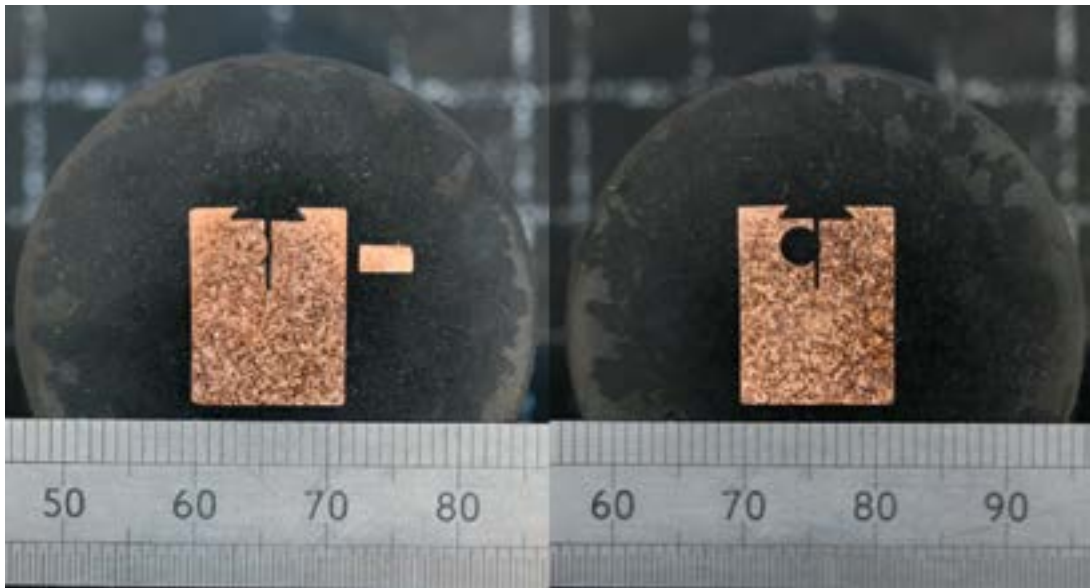


Figure 3-1. WOL A (LHS) and WOL B (RHS) prior to being cut out of Bakelite.

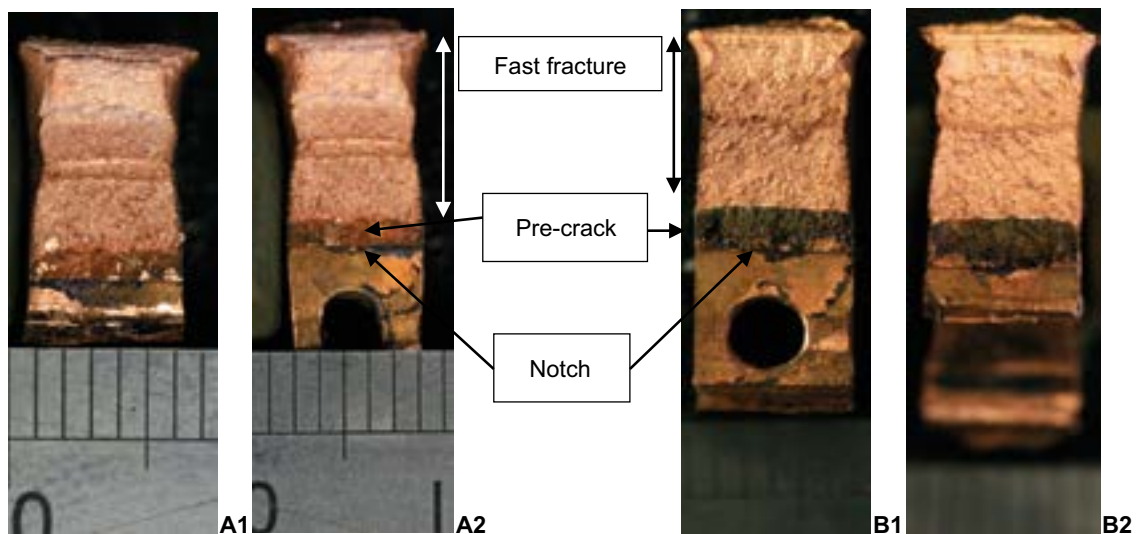


Figure 3-2. Photographic images of WOL A1 and A2, WOL B1 and B2 fracture faces post fatigue and fast fracture (scale 1 mm bars).

3.1.2 Confocal microscope images, visual features and average crack length of WOL fracture faces

Figure 3-3 and Figure 3-4 are Alicona confocal microscope images of each fracture face, showing further detail of the pre-machined notch, pre-crack area (i.e. the fracture surface of the pre-crack created by fatigue prior to the start of the experiment in the borehole) and fast fracture area (i.e. the area exposed when the specimens were fatigue-cracked open for examination after removal from the Bakelite mount). All fracture faces were imaged at $\times 2.5$ magnification. The double band in the fast fracture region is due to the softness of the material, which elongated in this area when being cleaved open. This did not affect the pre-crack area. There appears to be a shinier region at the end of the pre-crack area on WOL A and WOL B, with the shinier region being better defined on WOL B. SEM analysis of this area was carried out to investigate this morphology further. Other than the shinier region at the end of each pre-crack fracture face, and the fact that there appears to be heavier surface deposition (possibly oxide) on WOL B when compared with WOL A, there are no other discernible features of interest noted from Figure 3-3 and Figure 3-4.

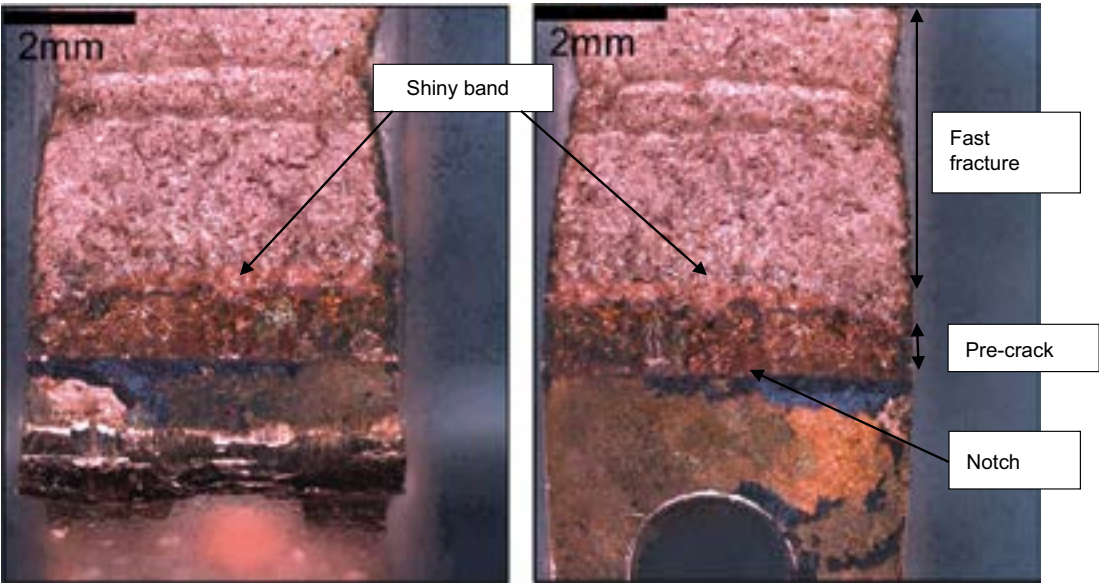


Figure 3-3. WOL A1 (LHS) and A2 fracture faces (RHS).

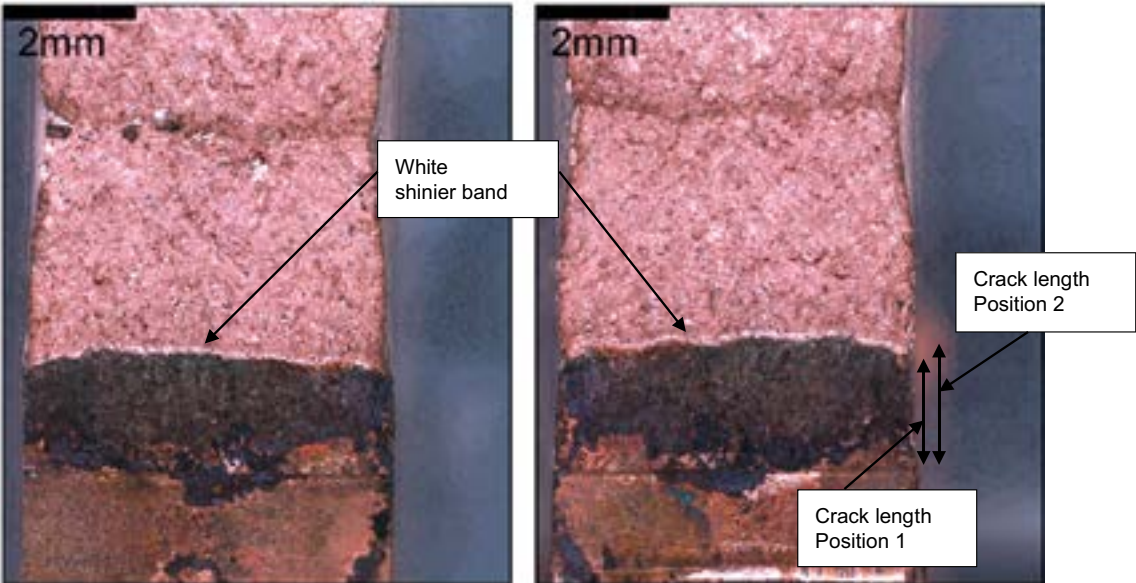


Figure 3-4. WOL B1 (LHS) and B2 (RHS) fracture faces.

Figure 3-5 is an example of the tilted 3D profile that the Alicona microscope is able to produce of an imaged surface. It shows that the dark deposition on the pre-cracked region had also deposited above the notch of the specimen. There is no evidence from the Alicona microscope images of any dark deposition on any other region past the pre-cracked region.

To obtain further analysis of the shinier bands at the end of the pre-crack using SEM, the average crack length was measured for each fracture face. The results are presented in Table 3-1, with crack lengths measured (from the notch) ranging from 935–1961 μm , depending on which fracture face was measured. The results imply that there is only evidence of a pre-crack with no other cracking present, when these lengths are compared against the pre-crack lengths measured during preparation of the WOL specimens (see Appendix A.1). The pre-crack requirement was to have a pre-crack length of 1.5 mm. Taking into account the fact that the true crack length from pre-cracking has a spread of several hundred microns, then a range of 935–1961 μm does not indicate crack elongation due to SCC in these specimens.

Table 3-1. Average crack lengths for WOL A1, A2, B1 and B2.

| | Crack length position 1 (pre-crack up to shiny band, μm) | Crack length position 2 (pre-crack and shiny band, μm) |
|--------|---|---|
| WOL A1 | 935 | 1250 |
| WOL A2 | 1025 | 1258 |
| WOL B1 | 1631 | 1714 |
| WOL B2 | 1862 | 1961 |

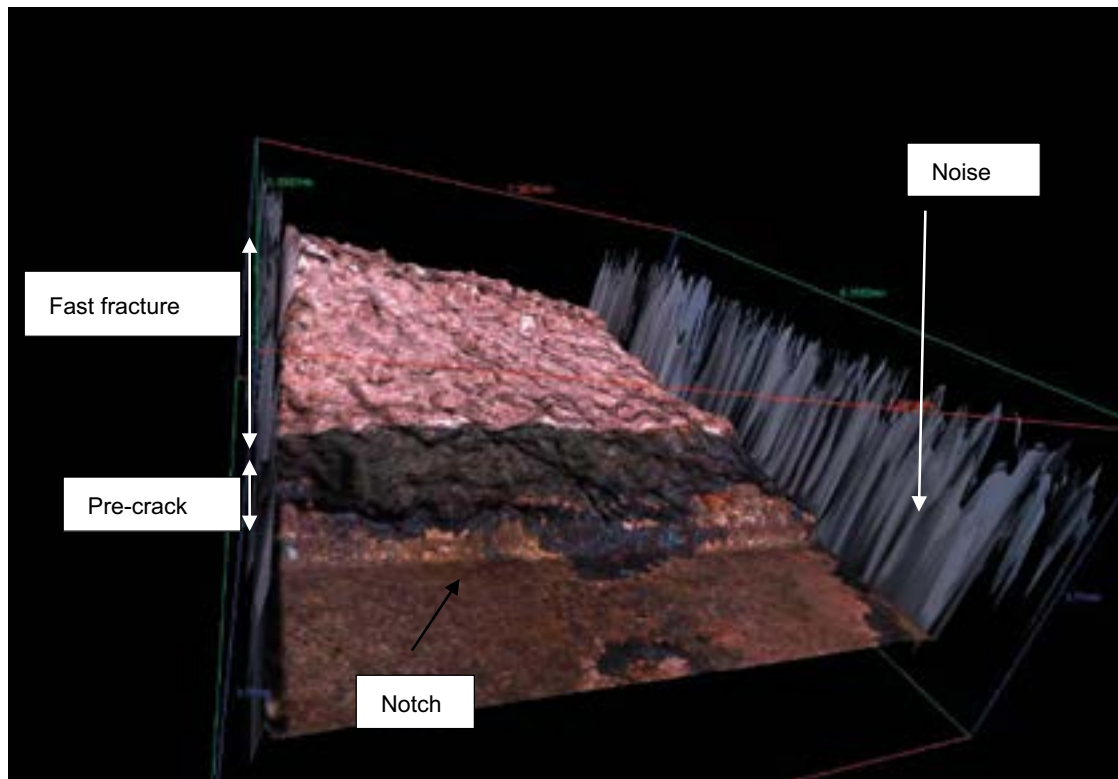


Figure 3-5. 3D image of WOL B1 fracture surface.

3.1.3 SEM (Scanning electron microscope) images of WOL fracture faces

Figure 3-6 to Figure 3-9 are combined secondary electron images of each notch, pre-crack and start of fast fracture areas of WOL specimens A1, A2, B1 and B2. It is not clear on fracture faces A1 and A2 where the pre-crack area ends, but on the B1 and B2 fracture faces the pre-crack end position is shown distinctly by the change of surface morphology from rough and dark to a much smoother and lighter band (shinier). The SEM did not clearly show the pre-crack and fast fracture regions on the WOLA fracture faces but it was better defined on the fracture faces of WOL B, as labelled. Figure 3-4 shows that there is a pre-crack region, a shiny region and then a fast fracture region on the open faces of WOL B. The two lengths measured in Table 3-1 are firstly the average length of the pre-crack up to the shiny band. The second average length is the sum of the pre-crack and the shiny band.

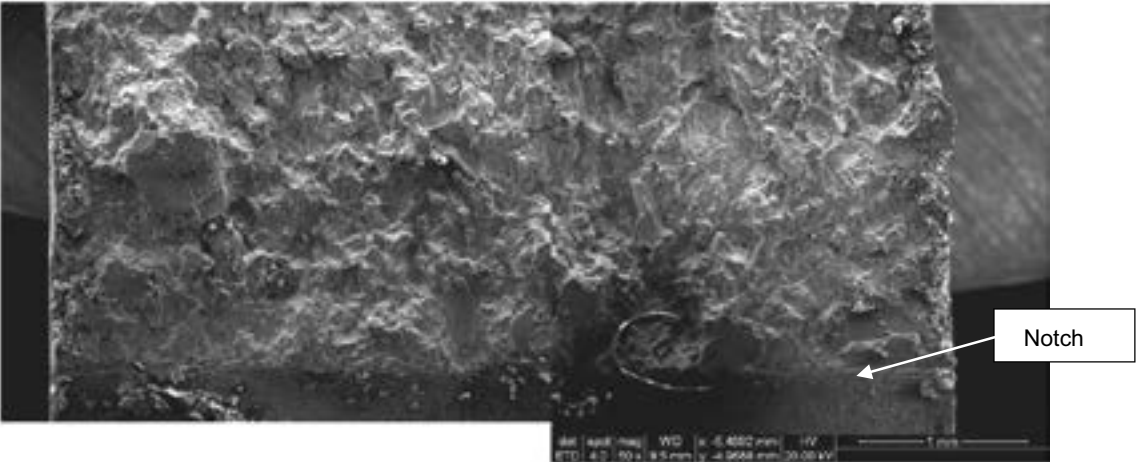


Figure 3-6. SEM image of WOL A1 (near to cage).

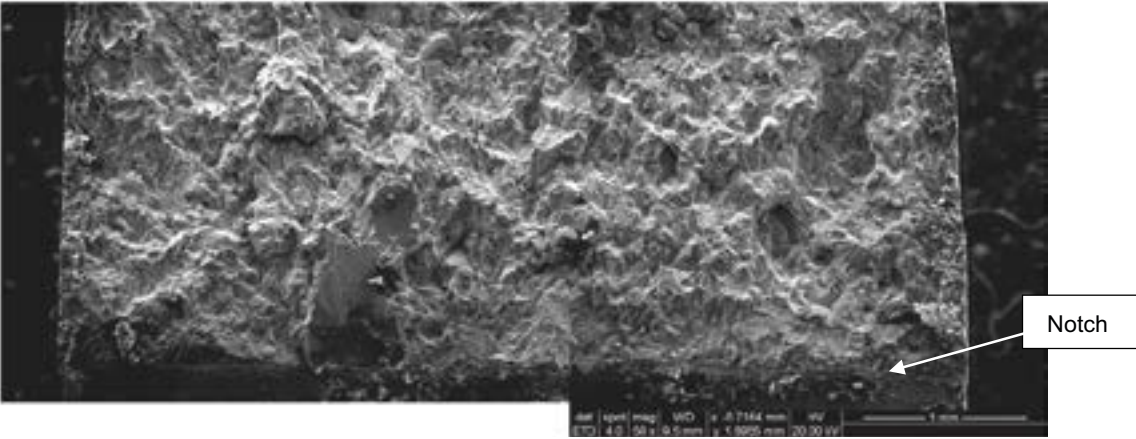


Figure 3-7. SEM image of WOL A2 (near to cage).

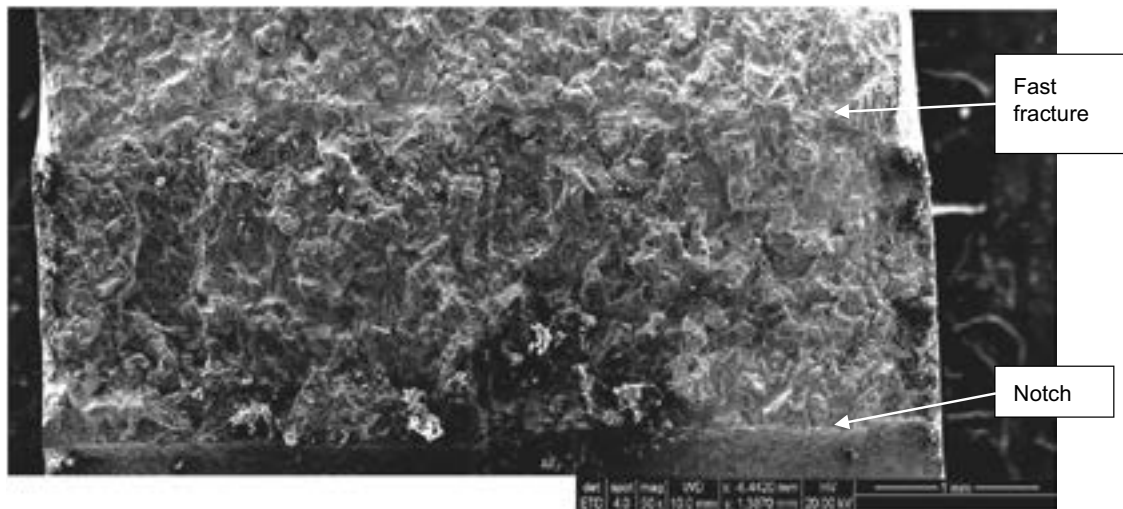


Figure 3-8. SEM image of WOL B1 (near to borehole flange).

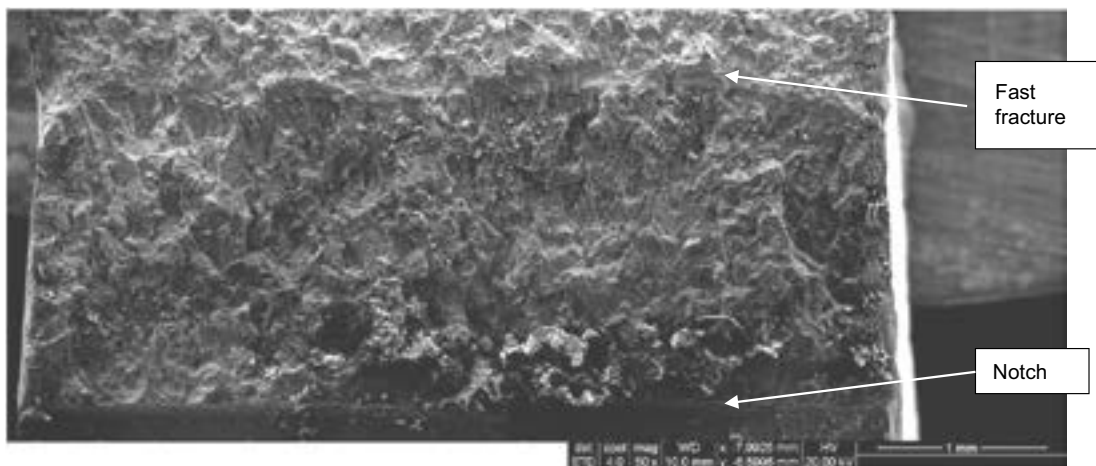


Figure 3-9. SEM image of WOL B2 (near to borehole flange).

Higher magnification images (Figure 3-10 to Figure 3-12) of WOL B1 and B2 show the location of the shinier band, as seen on the Alicona images in the previous section. The shinier band consists of fatigue lines and smoothed regions, where the initial stages of pulling open the WOLs occurred. This initial smoothing of the fast fracture region is due to the technique required to open the specimens. This shinier band is an artifact that was not caused by the test conditions. There is no evidence of any crack growth that could be attributed to SCC from the pre-crack. The presence of the dark deposit on the surface of each pre-crack surface partially hindered a full analysis. EDX (energy dispersive X-ray spectroscopy) of the pre-crack and fast fracture regions as shown in Figure 3-13, Figure 3-14 and Table 3-2 show that there is evidence of an oxygen-containing deposit being present on the pre-crack area and negligible oxide being present on the fast fracture region. Table 3-2 also indicates the presence of some carbon in the deposit. Due to the limited sensitivity of the EDX technique it can only be speculated that the carbon is present as an organic deposit or as carbonate (when taking into consideration the EDX results for the U-bend specimens, Section 3.2.3). Therefore, although visual evidence of a deposit on fracture faces A1 and A2 is limited to SEM images, the EDX analysis supports the conclusion from the Alicona images of there being an oxygen-rich deposit present only on the pre-crack area and no further.

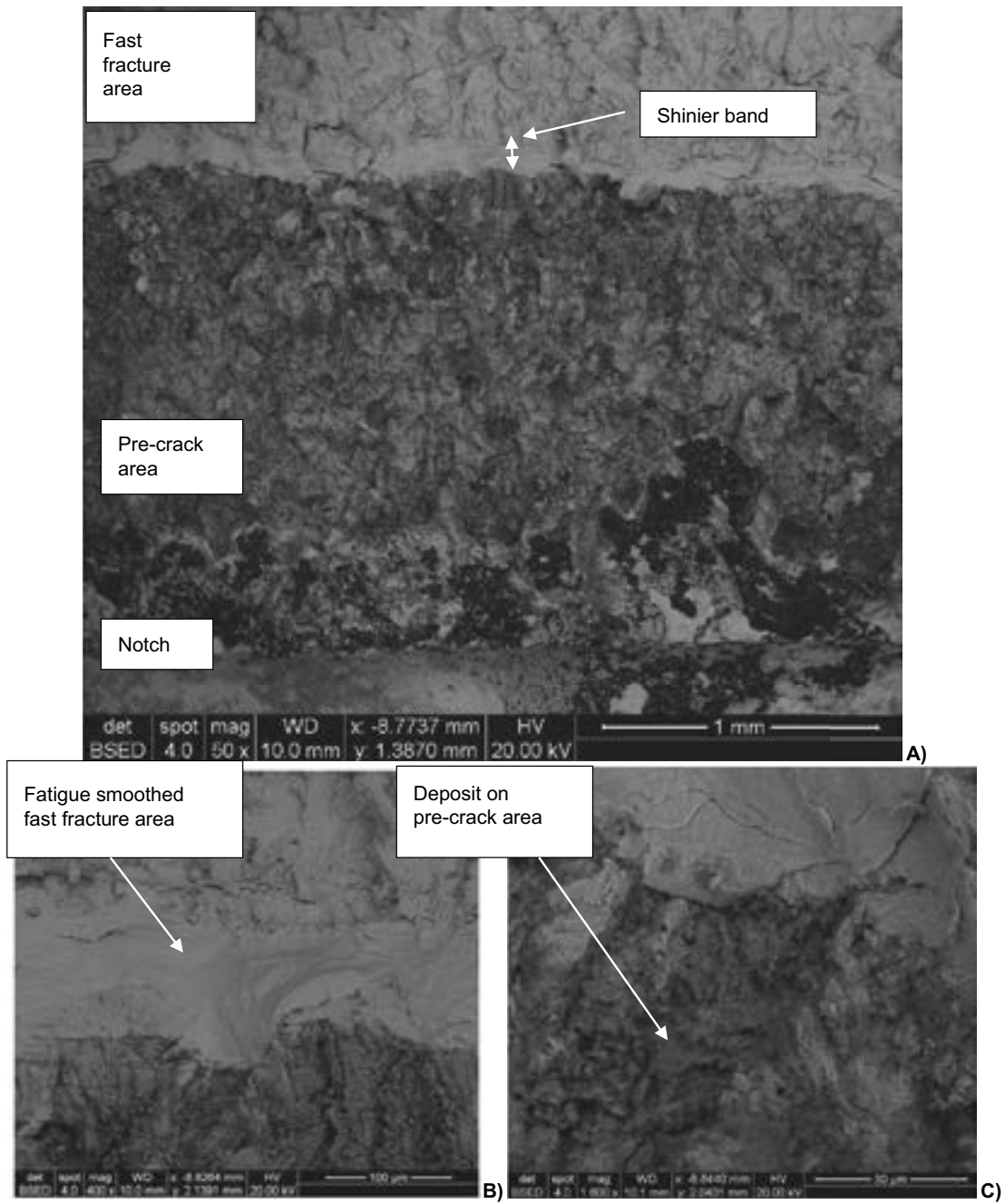


Figure 3-10. SEM image of WOL B1 (near to borehole flange), end of pre-crack, A) $\times 50$, B) $\times 400$ and C) $\times 1600$ magnification.

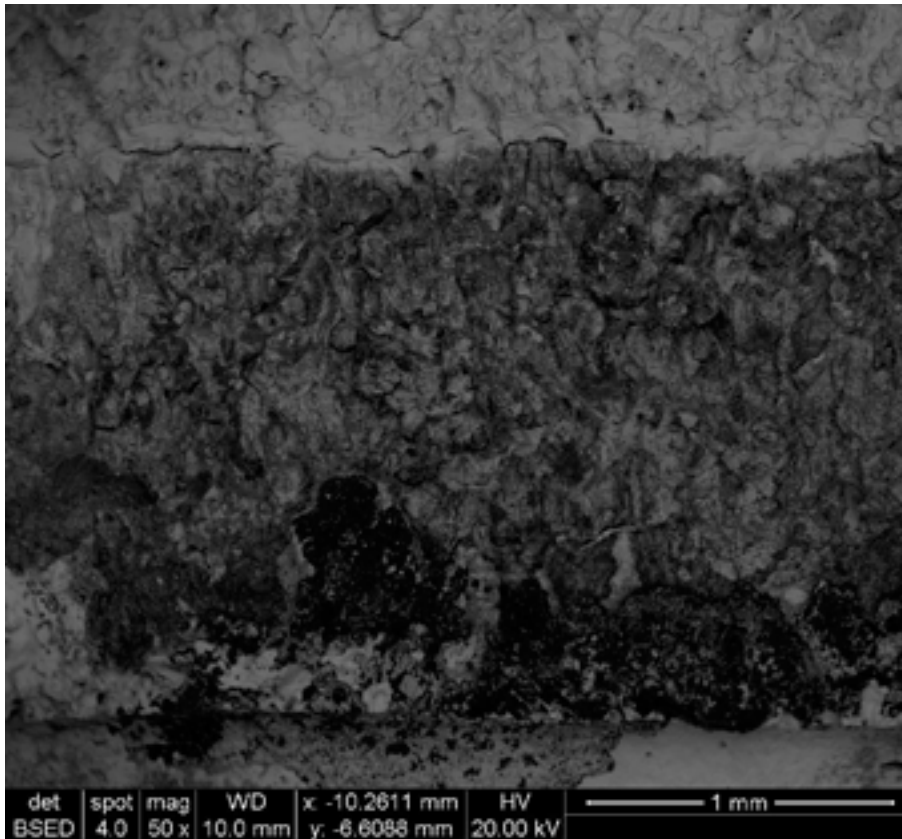


Figure 3-11. SEM image of WOL B2 (near to borehole flange), end of pre-crack, ×50 magnification.

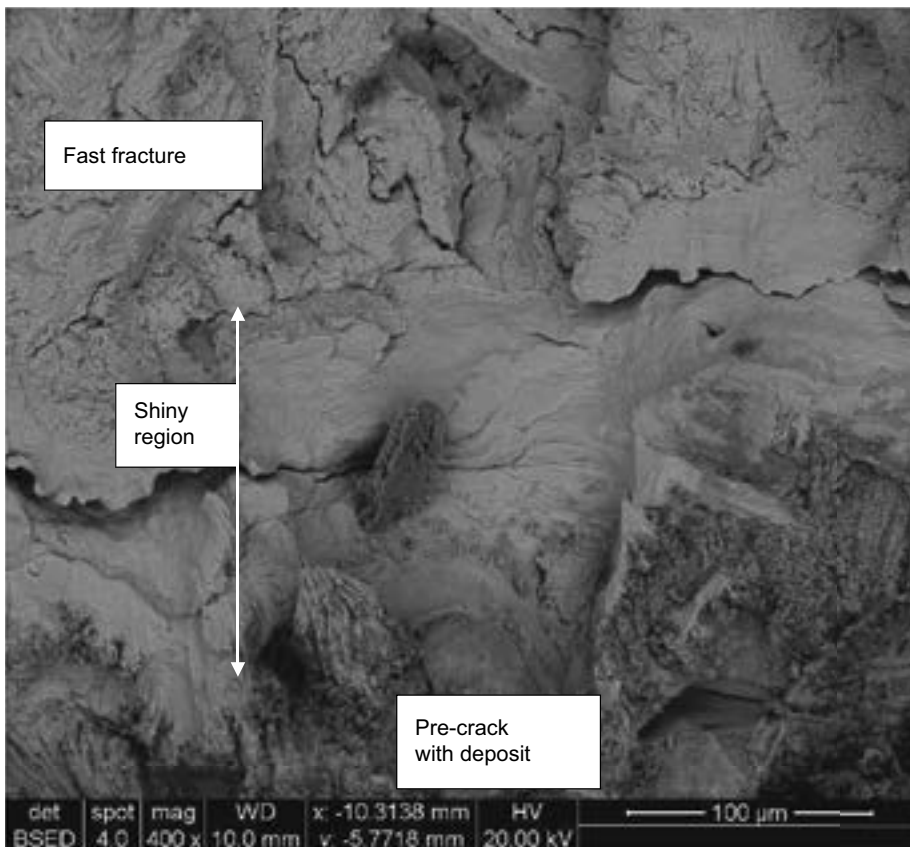


Figure 3-12. SEM image of WOL B2 (near to borehole flange), end of pre-crack, ×400 magnification.

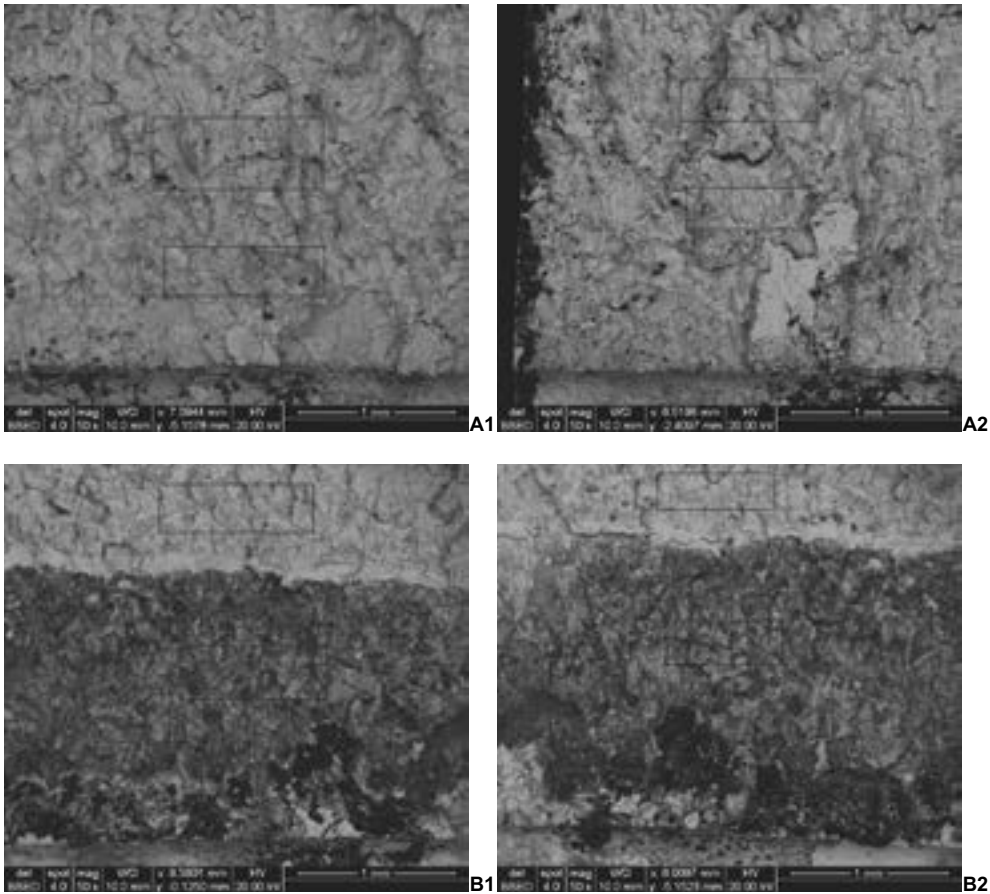


Figure 3-13. Backscattered electron detector (BSED) images of pre-crack and fast fracture regions showing positions of EDX analysis for oxygen (oxide) determination on WOL A (top row) and WOL B (bottom row) surfaces.

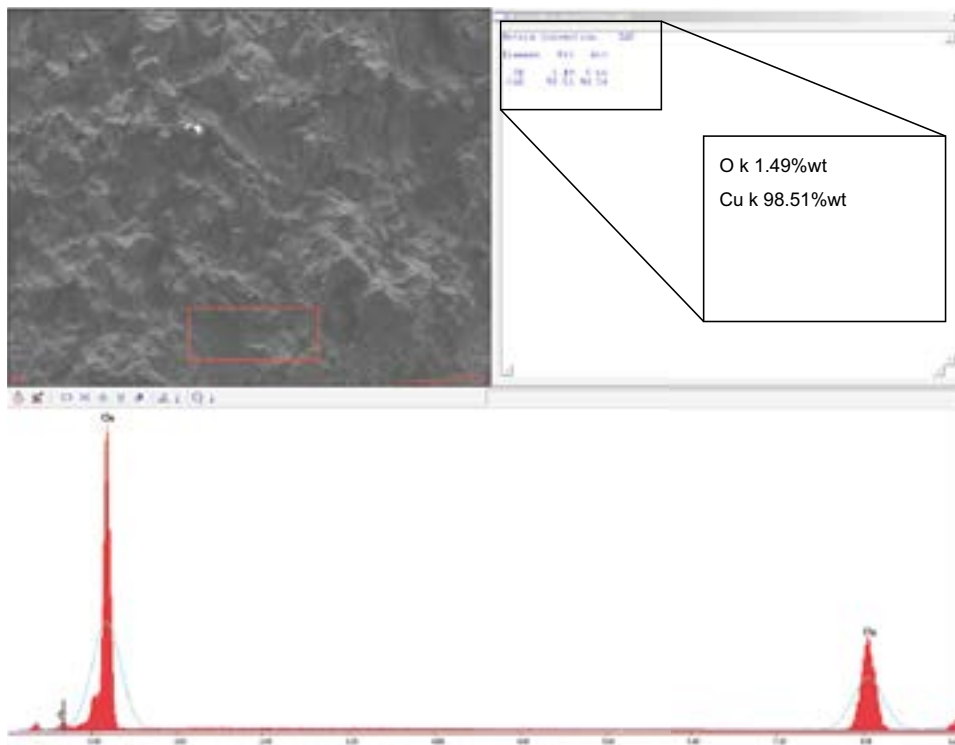


Figure 3-14. Example of EDX analysis for pre-crack region of WOL specimen A1.

Table 3-2. EDX values for all WOLs in pre-crack and fast fracture region.

| WOL fracture | Pre-crack Oxygen % | Pre-crack Copper % | Fast fracture Oxygen % | Fast fracture Copper % |
|--------------|--------------------|--------------------|------------------------|------------------------|
| A1 | 1.49 | 98.51 | 0 | 100 |
| A2 | 7.17 (C16.42) | 76.41 | 0.68 | 99.32 |
| B1 | 15.36 | 84.64 | 1.64 | 98.36 |
| B2 | 16.35 | 83.65 | 1.98 (C 5.25) | 92.17 |

3.1.4 Conclusions from examination of WOL specimens

The two WOLs broken apart to analyse the fracture faces showed that there was no evidence of crack elongation due to SCC; however there was a dark oxygen-rich deposit on the pre-crack and partially above the notch on all the fracture faces. The density of the deposit on the pre-crack area was more marked on the WOL B fracture faces than on the WOL A specimen; however Alicona microscope imaging and EDX elemental analyses confirmed the presence of the deposit on all pre-cracked areas (i.e. for A1, A2, B1, and B2). The shinier bands evident in the Alicona microscope images are regions of physical interaction between the two faces as the specimens were being cracked open. In addition, the applied local stress may have induced plastic strain in the shiny light coloured band.

3.2 U-bend specimens

3.2.1 Photographic images of U bend specimens

In order to determine, and possibly distinguish between, the effects of in situ exposure in the MiniCan test and the effects of mechanical stress (if any) during preparation (i.e. bending) of the U-bend specimens, a strip of copper of similar dimensions (0.5 mm thicker) was bent into a U-bend using the curvature of the tested U-bends as a template (Figure 3-15). The copper strip was bent around a former, with no external heat applied, then bolted in tension. This procedure was carried out using the same approach as that used for the U-bend specimens that had been prepared in 2006 and used in the in situ test. The aim of comparing an untested U-bend with the tested U-bends was to determine whether any surface features could be attributed to the mechanical forming of the U-bend. Although it is not clearly evident, there appears to be an “orange peel” effect on the surface of the untested U-bend (Figure 3-15). An orange peel effect is clearly visible on U-bend specimens 95UG and 94UG (Figures 3-16 and 3-17). Further evidence of the orange peel effect is presented in the following section.

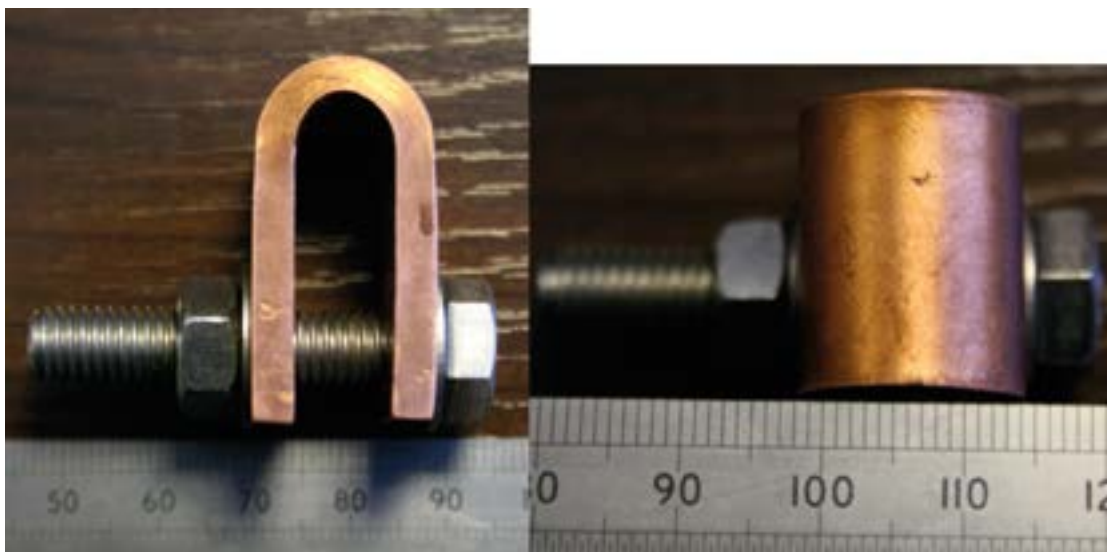


Figure 3-15. Side view and top view of untested U-bend copper specimen created for comparative analysis.

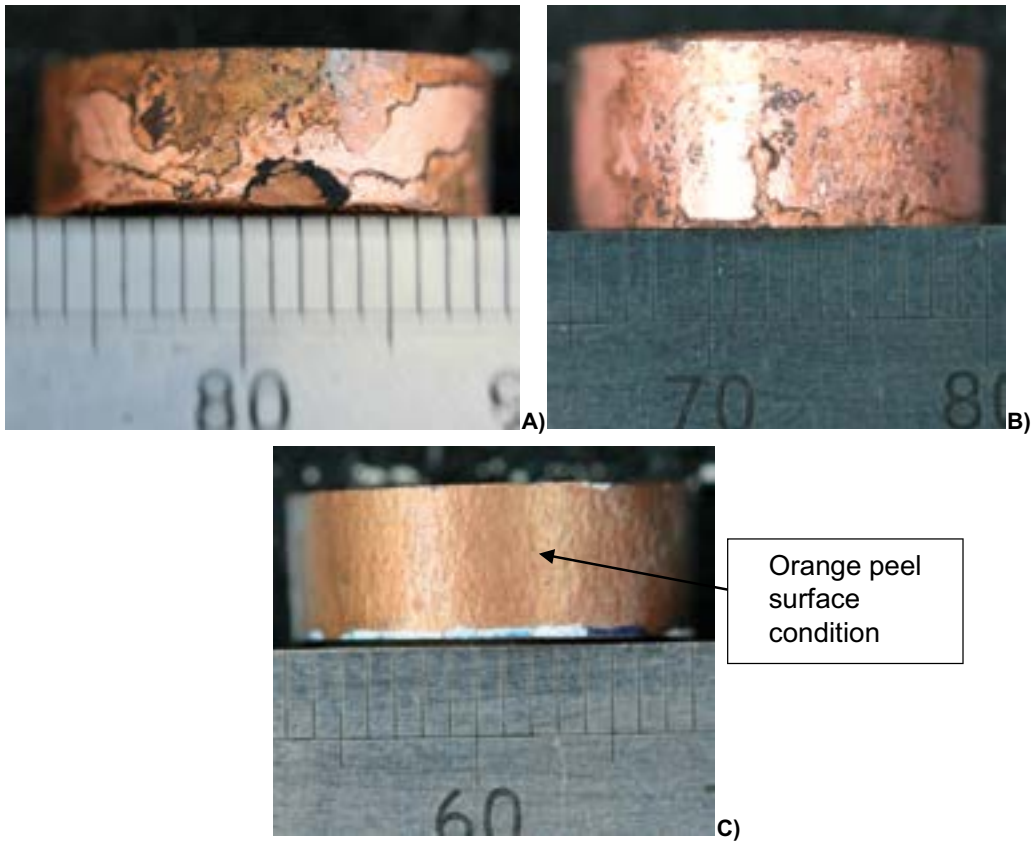


Figure 3-16. Surface condition of previously mounted slices A) bottom slice B) top slice and C) unmounted slice of 95UG (near to borehole flange).

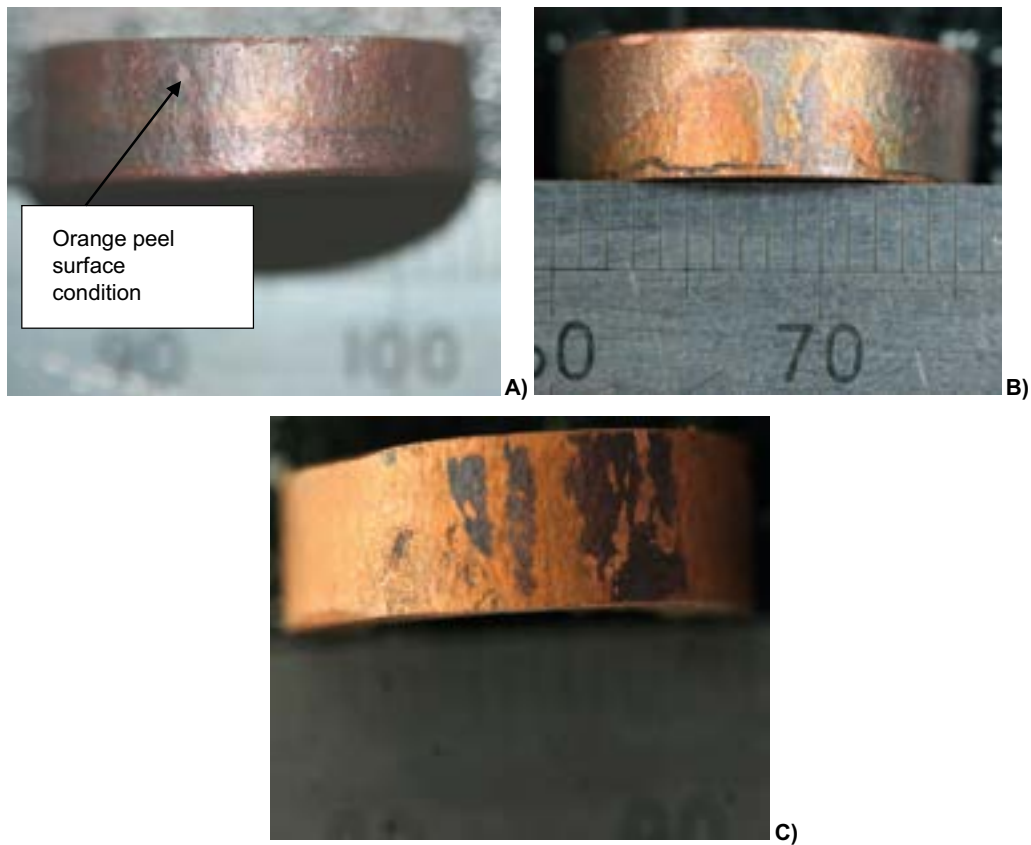


Figure 3-17. Surface condition of previously mounted slices A) bottom slice B) top slice and C) unmounted slice of 94UG (near to cage).

The term “orange peel” is an industrial term applied to non-uniform strain deformation across a material (ASM 1994). The undulating surface is caused by regions or grains deforming at different rates with respect to a neighbouring region or grain when a strain is applied to the material. It is commonly known for copper-based alloys with a large grain size. The undulating surface condition seen on the U-bend specimens from the MiniCan experiment is unlikely to have occurred during the experiment. There is a possibility that general corrosion may have occurred to further define any peaks and troughs of the undulating surface. This is due to strain variations between neighbouring grains, which can influence the rate of corrosion of individual grains.

In Figure 3-16 and Figure 3-17, showing the tested U-bends, there appears to be a residue or deposit on the surface of the U-bends. This is located on the inner, outer and flat end surfaces of the U-bends. The patchiness of the residue or deposit on the previously mounted sections / slices (top and bottom) is attributed to the removal of the Bakelite to re-evaluate the surface features of the U-bends. This is confirmed by the shininess of the patchy regions where fresh copper surfaces had been exposed.

3.2.2 Confocal microscope images, surface roughness (Ra) and visual features of U-bend outer surfaces

This section covers further analysis of the surface condition to determine whether exposure to the test environment had affected the overall state of the U-bends. Table 3-3 and the following images (Figure 3-18 to Figure 3-26) show that the surface condition (as stated above) had an undulating appearance resulting from straining the material when it was formed into a U-bend. This conclusion is further supported by Table 3-3, which gives the linear roughness values for each slice (see Appendix A.2 for the equation defining Ra). Linear roughness refers to the degree of roughness in the surface measured along an arbitrary straight line; the results are presented in terms of Ra, which is defined as the arithmetic average of the absolute values of roughness (ISO 1302:2002). The surface roughness of the flat ends was very low (~2 µm), whilst the average surface roughness of the U-bend sections (treated and untreated) was approximately 9 µm. The anomaly of the 95UG top slice value of 4 µm Ra can be attributed to either the presence of a smooth deposit or some residual Bakelite still being attached to the surface of this section.

The apex values of the surface roughness of the untreated U-bend compared with the tested U-bends from the MiniCan experiment show that the surface condition had been altered by general corrosion (assuming the specimens deformed in a similar manner). This is shown by comparing the specimen slices from 94UG and 95UG with the untreated U-bend Ra values. Surface roughness values were taken across approximately the same lengths across each specimen slice and over a length of at least five repeating unit lengths, in accordance with ISO standard practice for surface roughness measurements (ISO 1302:2002, ISO 4287:1997).

Table 3-3. Surface roughness of each U bend section across outer surface: apex of U-bend unless otherwise stated.

| Specimen Section | Ra (µm) |
|--------------------------|---------------------|
| Unmounted U bend 94UG | 7.936 |
| Top slice U bend 94UG | 10.362 |
| Bottom Slice U bend 94UG | 8.399 |
| Flat end 94UG | 2.090 |
| Unmounted U bend 95UG | 10.906 |
| Top slice U bend 95UG | 4.914 black deposit |
| Bottom Slice U bend 95UG | 11.699 |
| Flat end 95UG | 2.488 |
| Untested not used U bend | 4.959 |

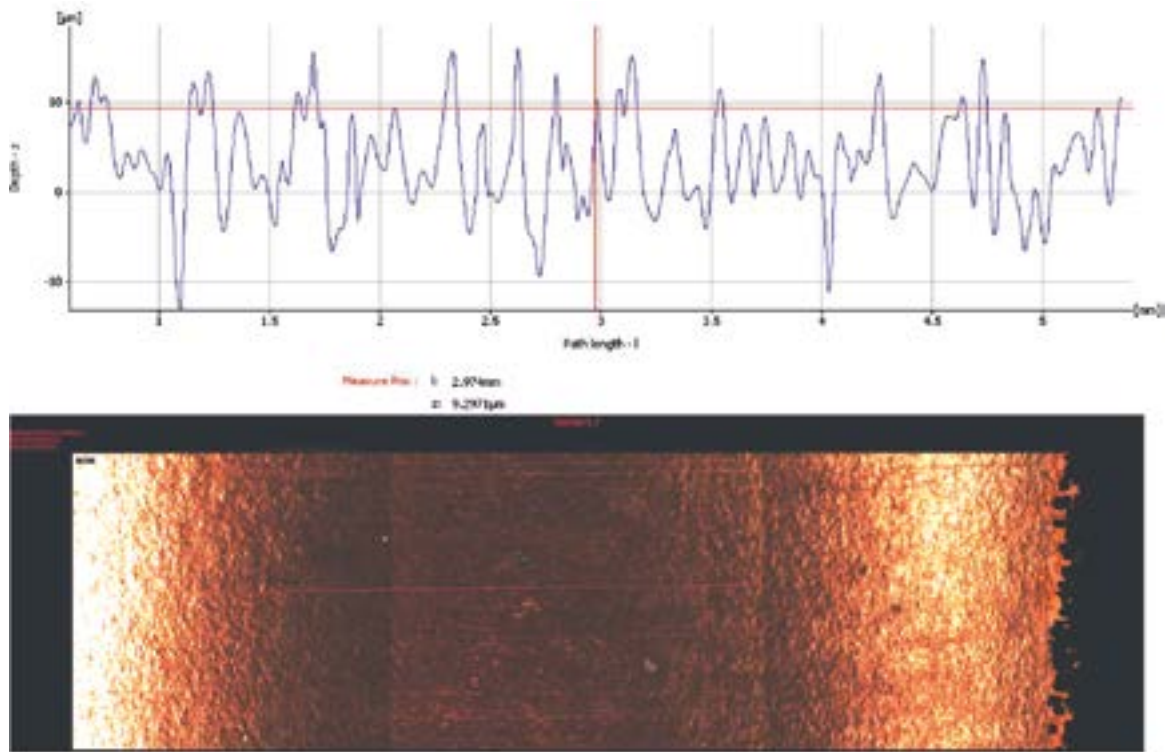


Figure 3-18. Surface roughness and optical microscopy image of apex of untested U-bend.

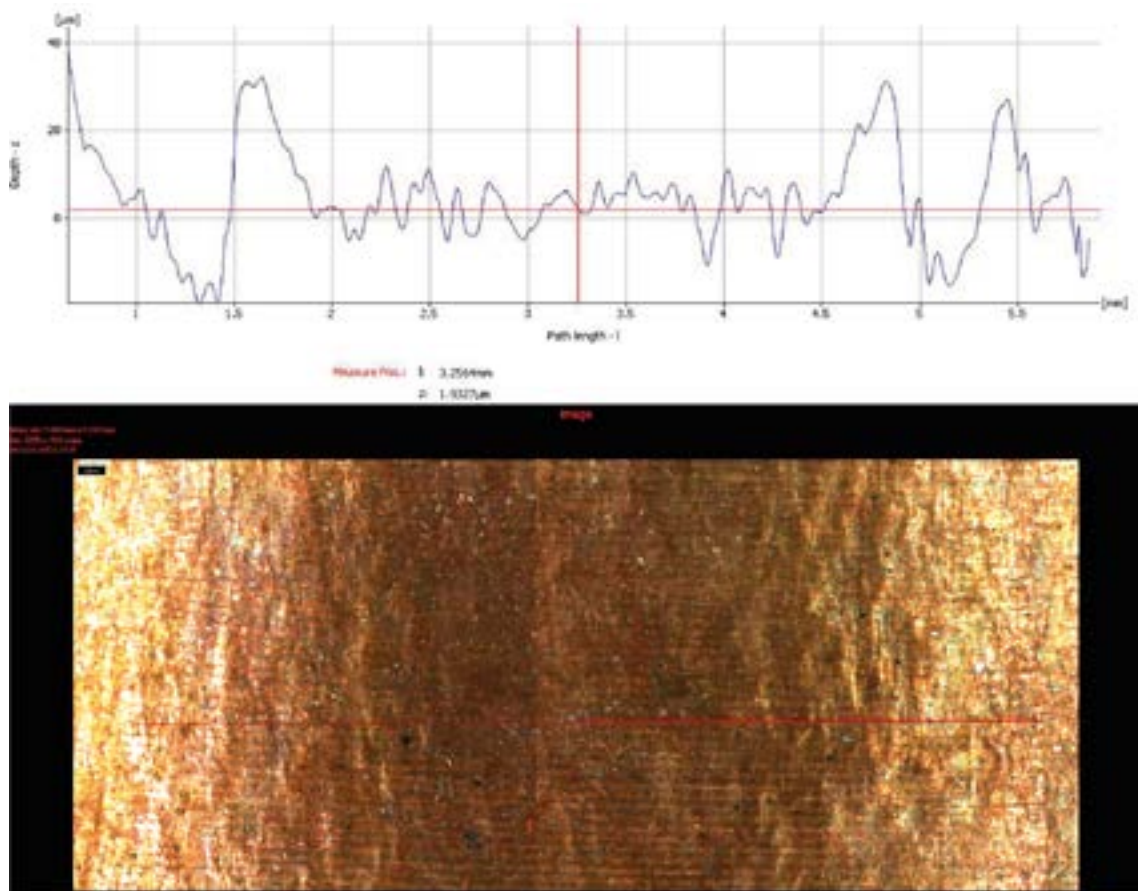


Figure 3-19. Surface roughness and optical microscopy image of apex of 94UG: unmounted slice.

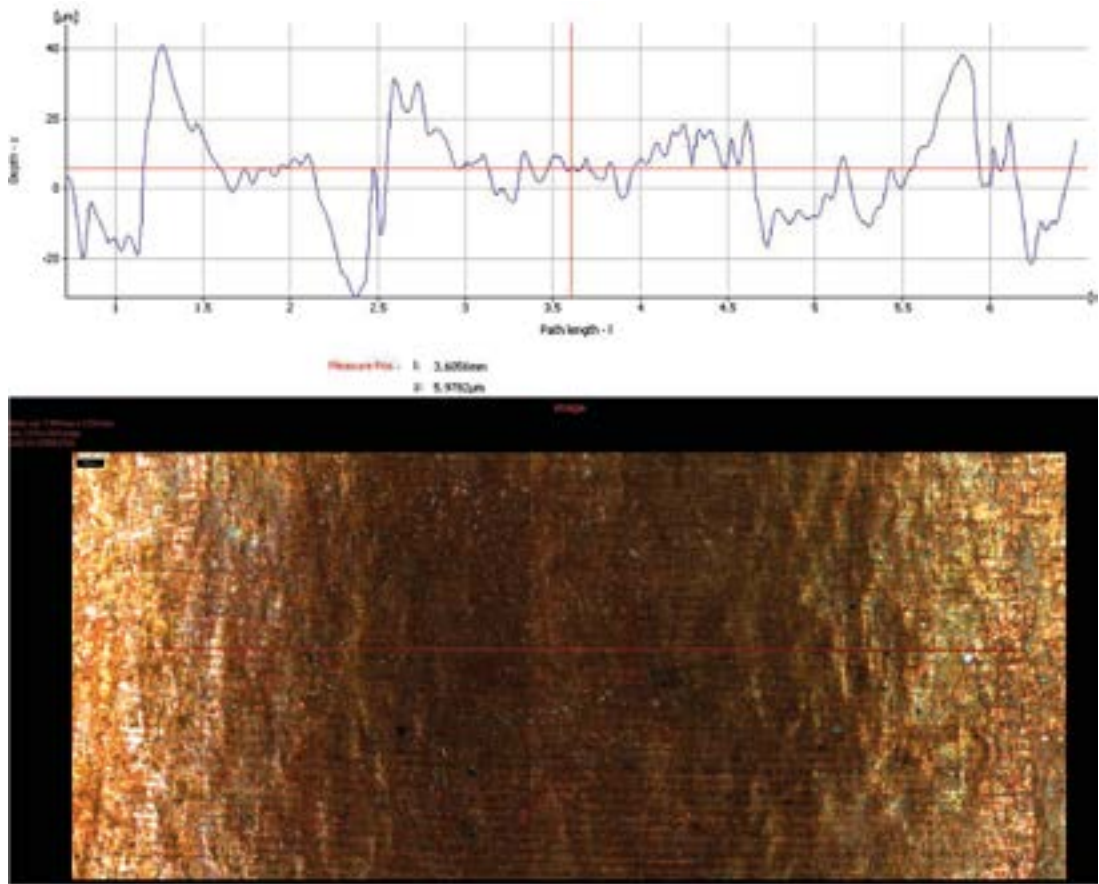


Figure 3-20. Surface roughness and optical microscopy image of apex of 94UG: bottom slice.

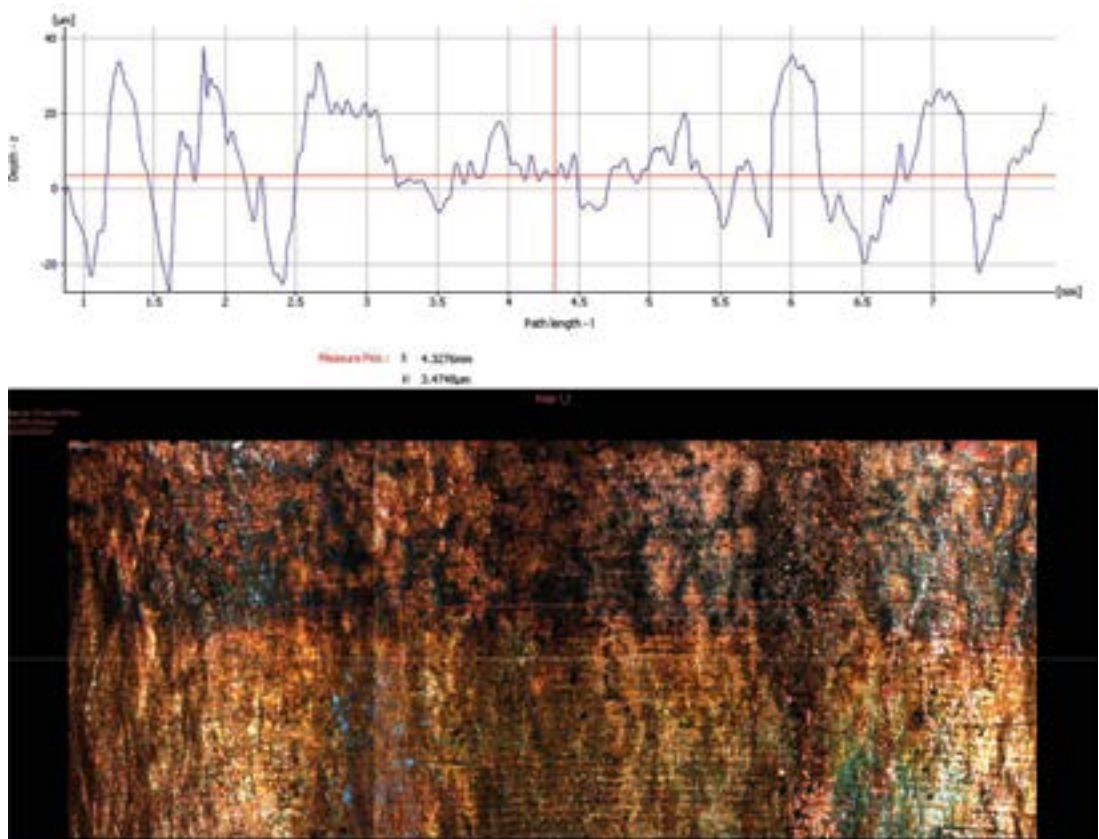


Figure 3-21. Surface roughness and optical microscopy image of apex of 94UG: top slice.

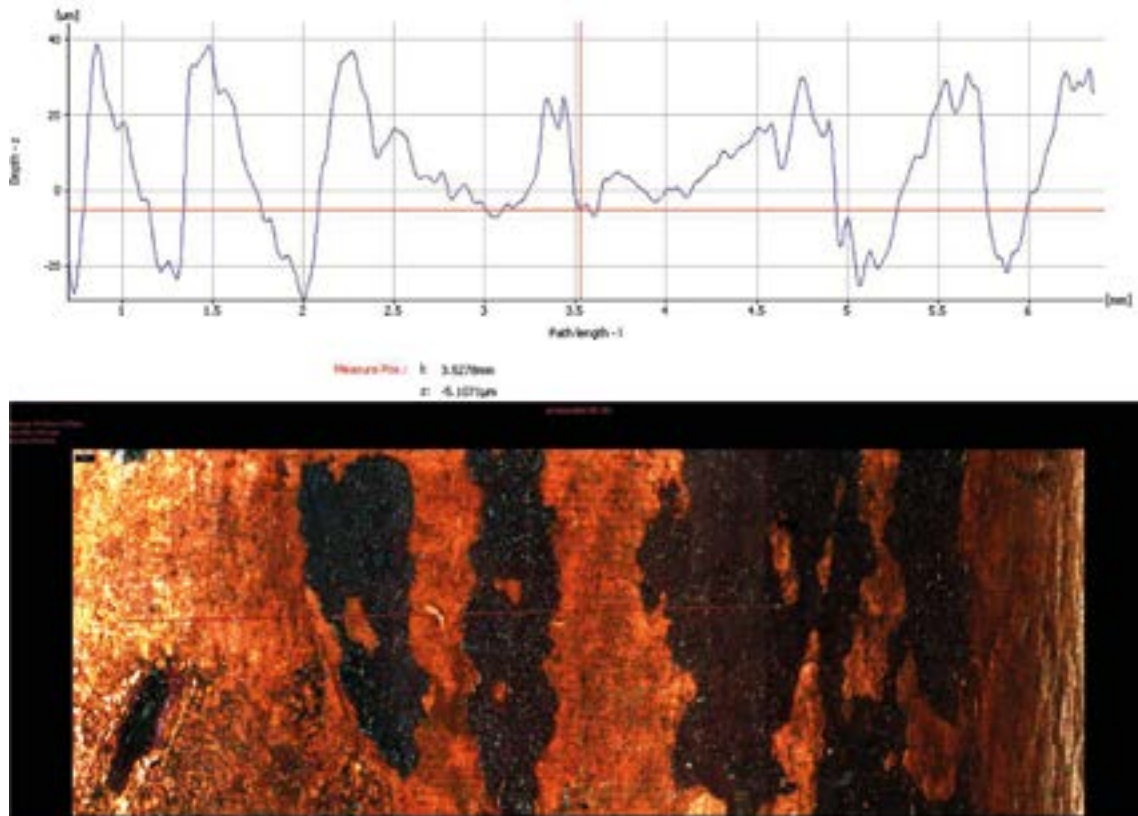


Figure 3-22. Surface roughness and optical microscopy image of apex of 95UG: unmounted slice.

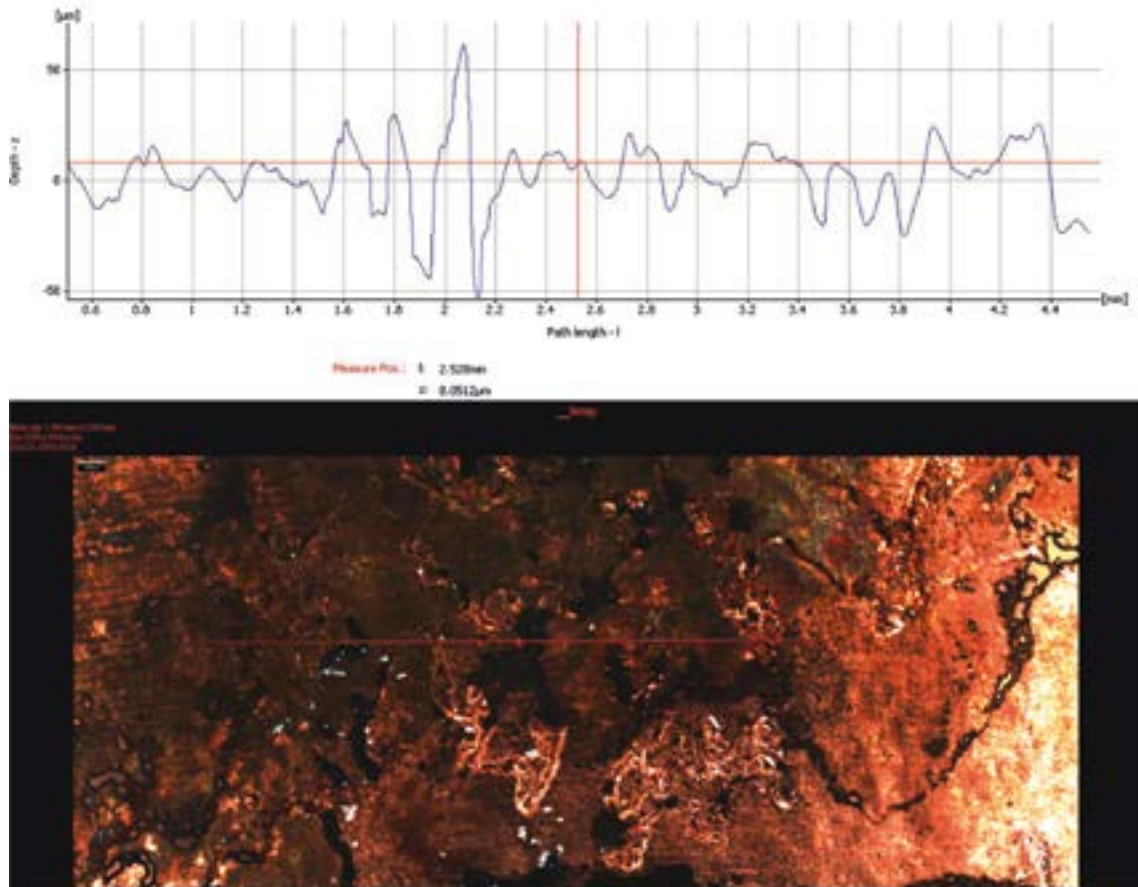


Figure 3-23. Surface roughness and optical microscopy image of apex of 95UG: bottom slice.

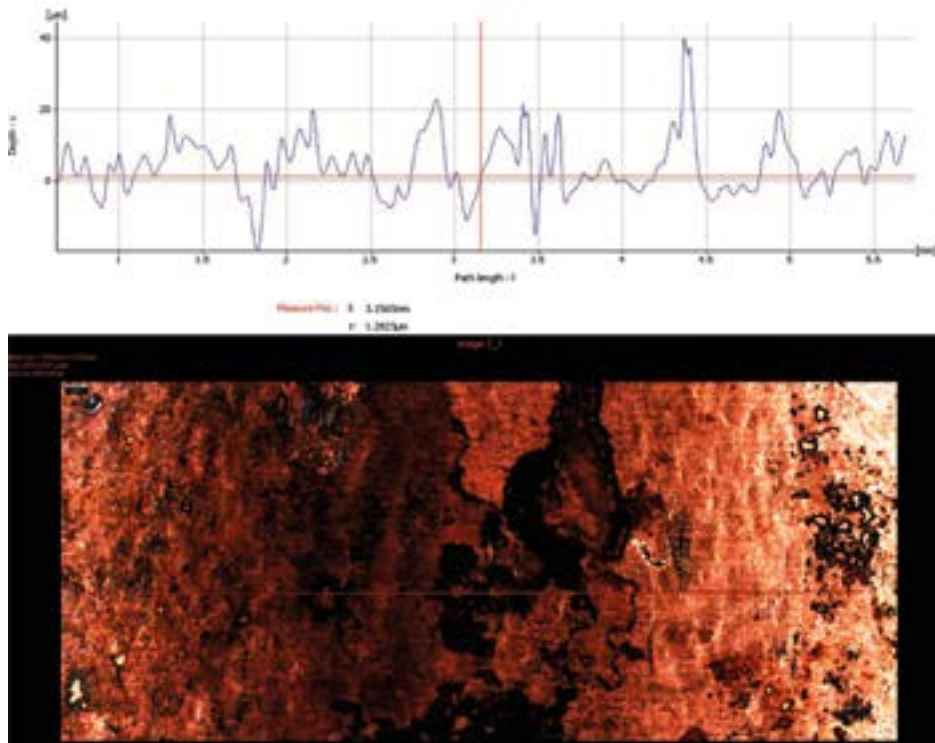


Figure 3-24. Surface roughness and optical microscopy image of apex of 95UG: top slice.

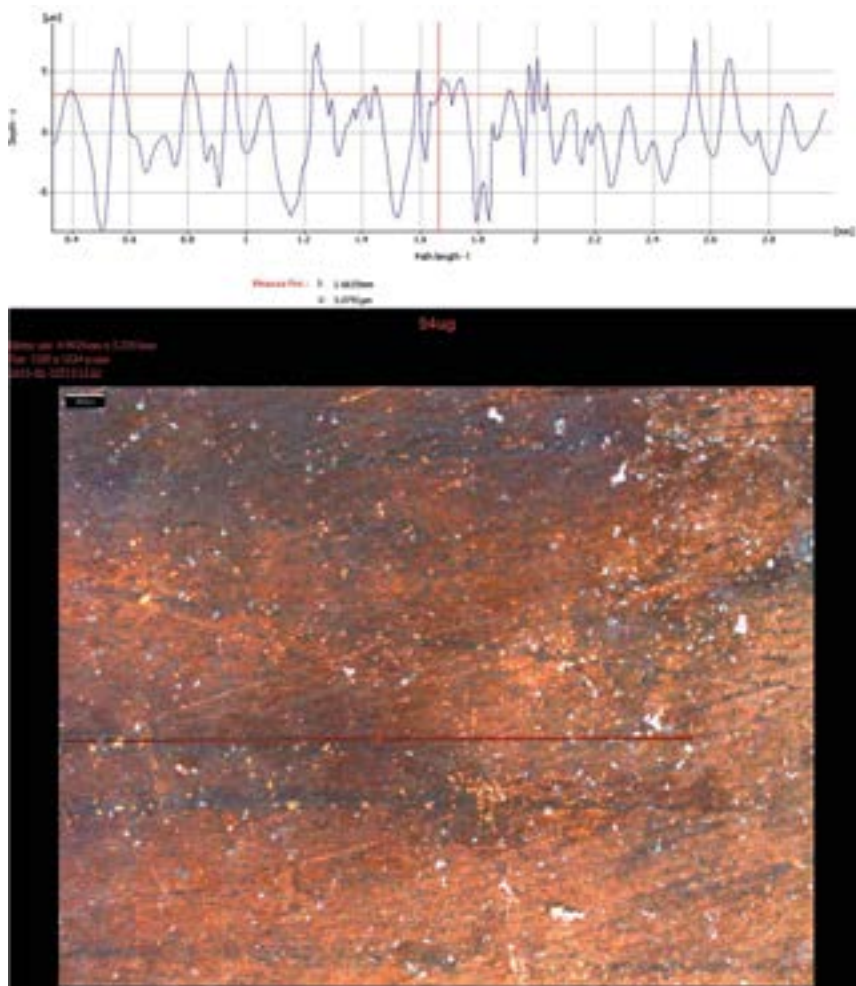


Figure 3-25. Surface roughness and optical microscopy image of 94UG: flat end of U bend.

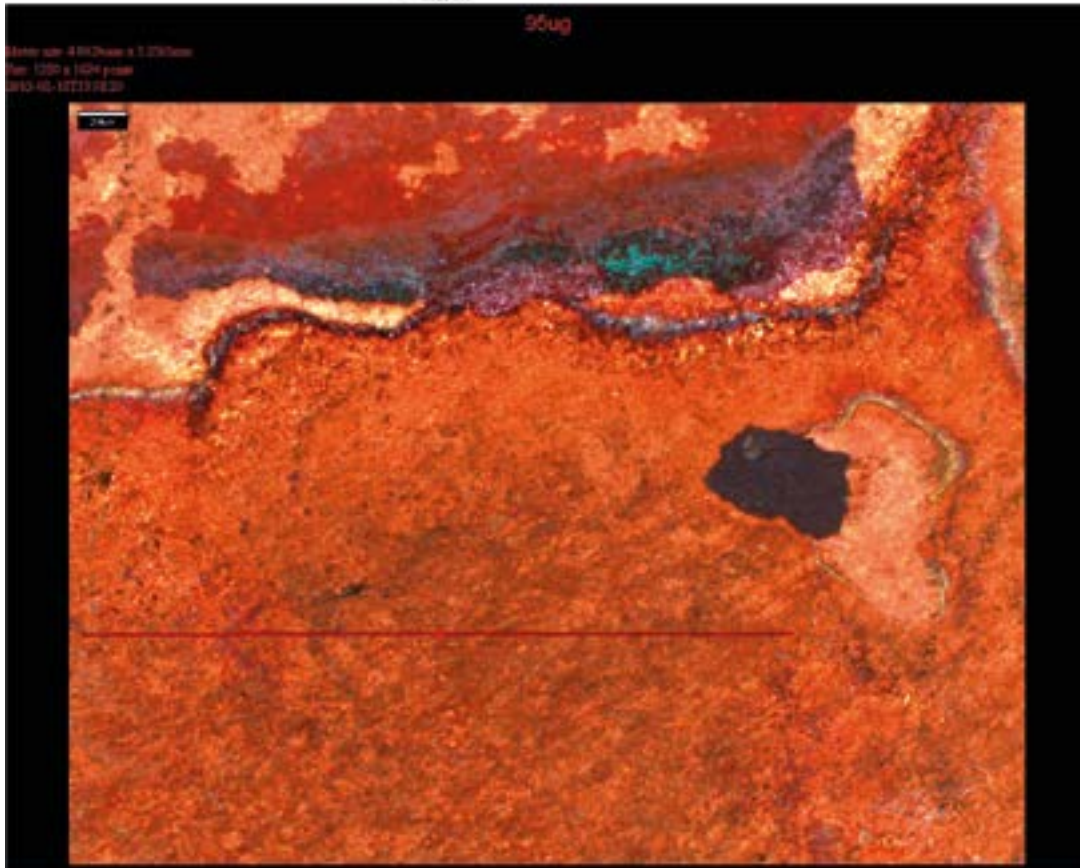
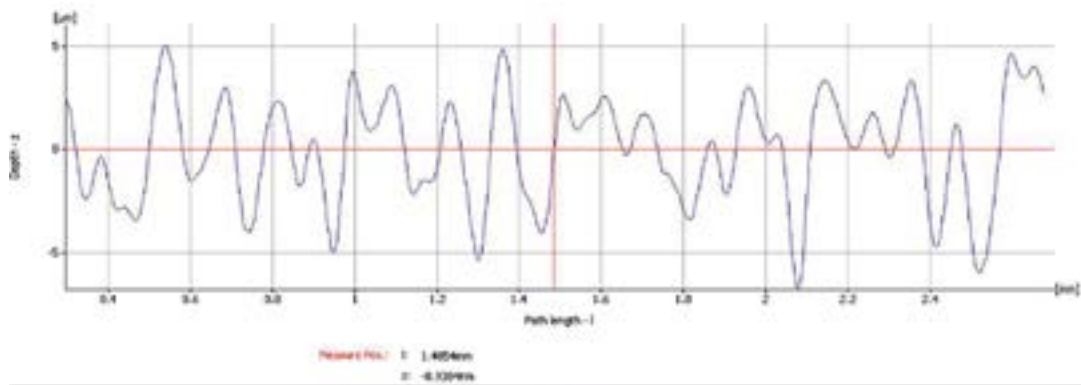


Figure 3-26. Surface roughness and optical microscopy image of 95UG: flat end of U-bend.

3.2.3 SEM microscope images and EDX (energy dispersive spectroscopy) analysis of U-bend surfaces

Figure 3-27 and Figure 3-28 show increasing magnification micrographs of the untested U-bend surface condition. It can be clearly seen in the higher magnification images that there are strain-directional striations and non-uniform surface features. These images are in agreement with the images above, showing non-uniform mechanical deformation of the apex of the U-bends.

Figure 3-29 to Figure 3-38 are SEM images of the tested U-bends, all showing evidence of surface deposition. Table 3-4 and Figure 3-29 show the results of EDX analyses at three different positions on the surface of a tested U-bend specimen whose elemental composition was characterised using EDX. All three positions showed the presence of carbon, oxygen, calcium and copper in varying proportions. This suggests that there was a general surface deposit that was oxygen-rich, possibly a calcium-copper carbonate. The pit size range seen on the surface was up to a maximum of ~20 μm diameter.

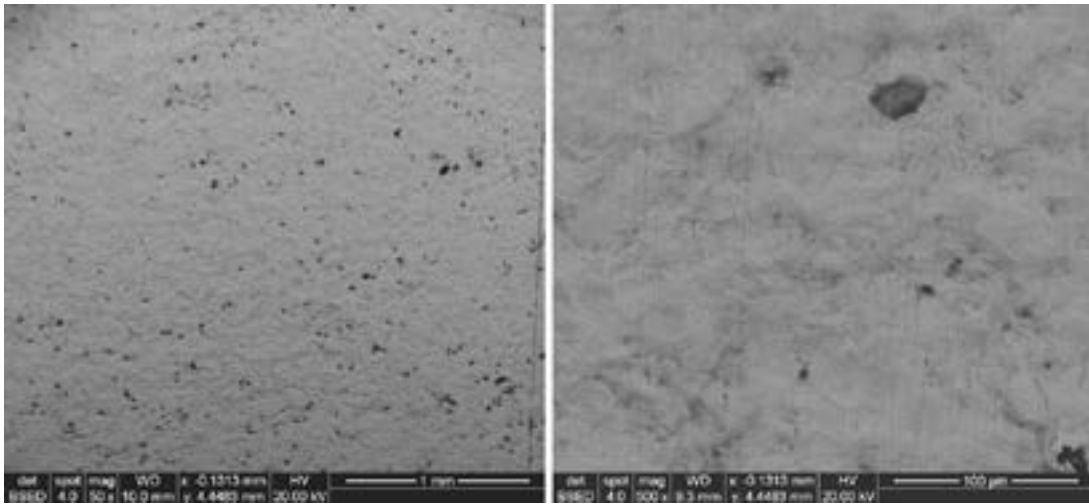


Figure 3-27. SEM images at $\times 50$ and $\times 500$ of untested U-bend.

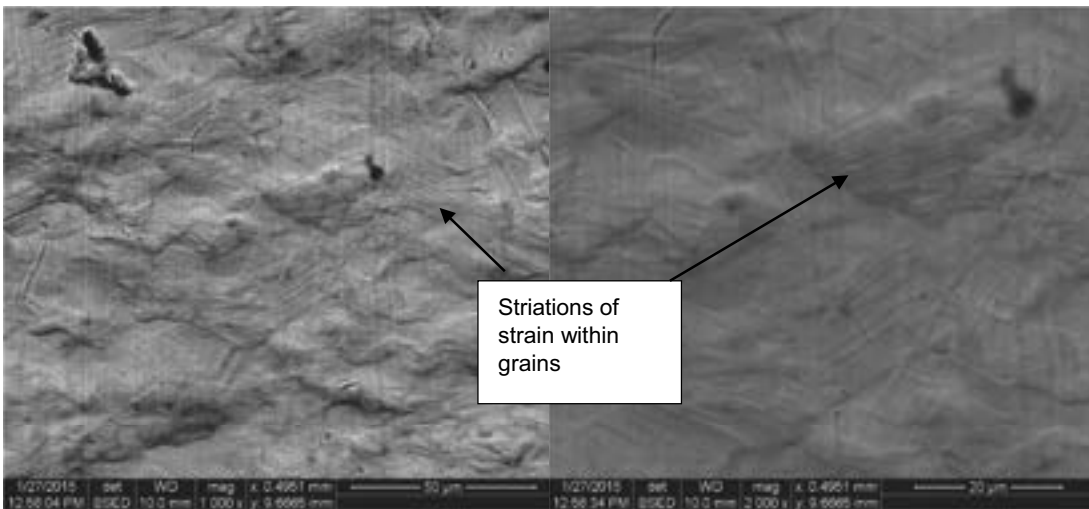


Figure 3-28. $\times 1000$ and $\times 2000$ magnification backscattered electron detector (BSED) images of untested U-bend with curvature from top of image to bottom.

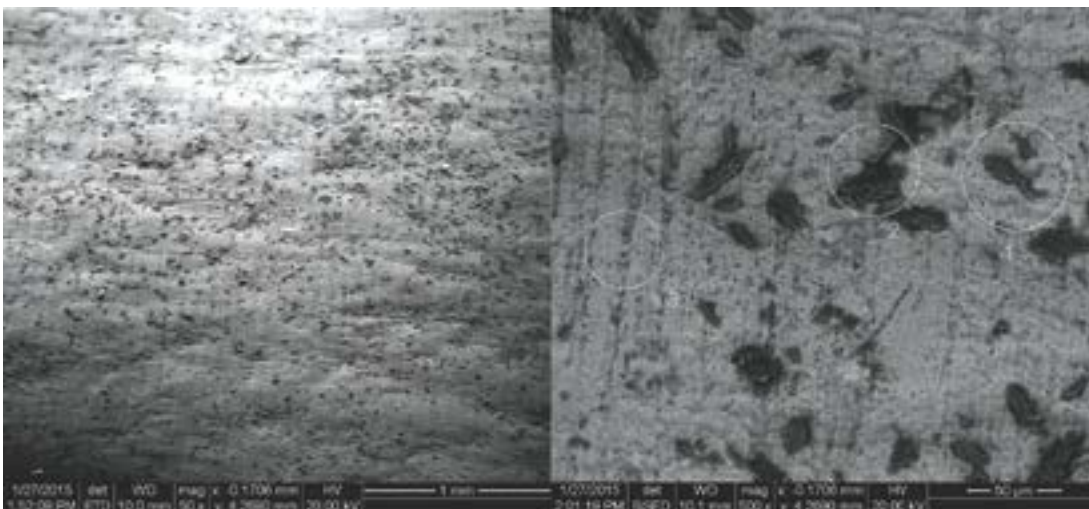


Figure 3-29. $\times 50$ and $\times 500$ magnification SEM images of 94UG unmounted section slice with curvature of U-bend from top of image to bottom. The results of EDX spot analyses of the features marked as 1, 2 and 3 are given in Table 3-4.

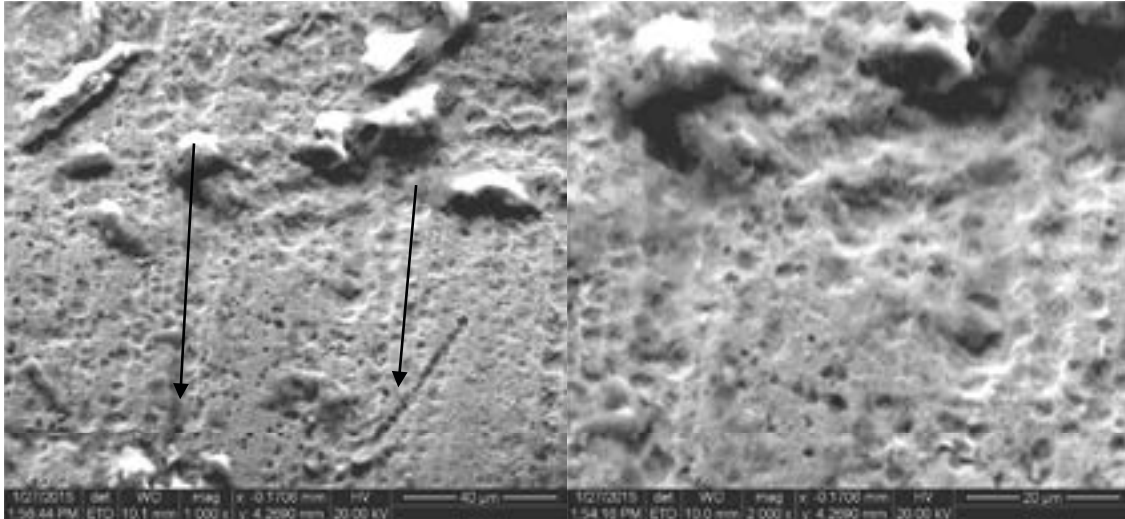
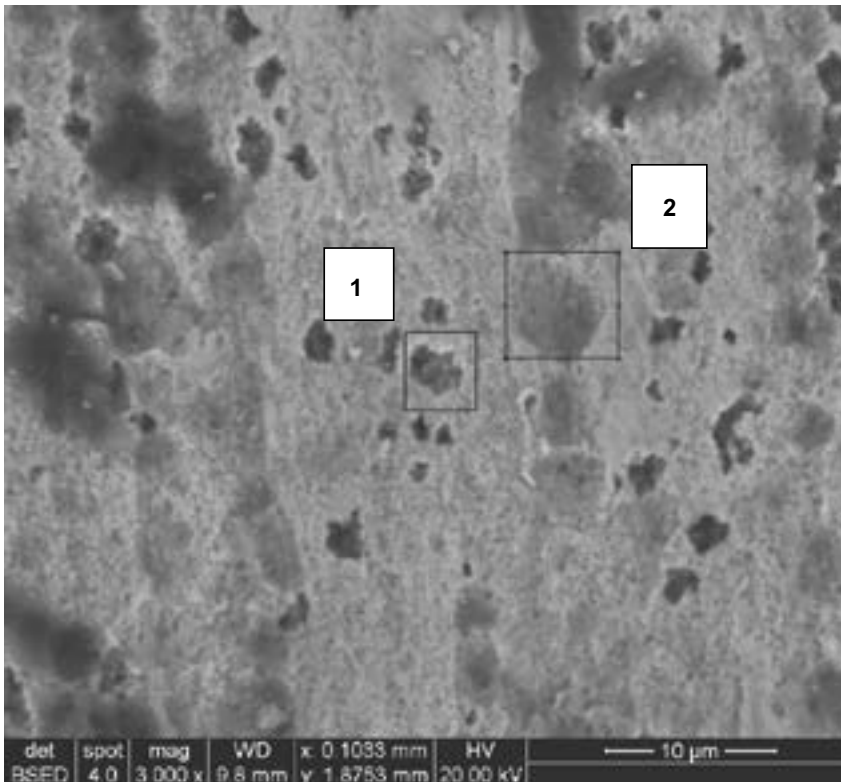


Figure 3-30. $\times 1000$ and $\times 2000$ magnification SEM images of 94UG unmounted section U-bend with curvature from top of image to bottom. Arrows denote tool mark directions.



| Element | Position 1 | Position 2 |
|----------------|------------|------------|
| Carbon | 34 | 43 |
| Oxygen | 8 | 6 |
| Copper | 55 | 51 |
| Other elements | 3 | - |

Figure 3-31. EDX analysis of pit 1 (general corrosion) and 2 (selective corrosion) of 94UG unmounted section.

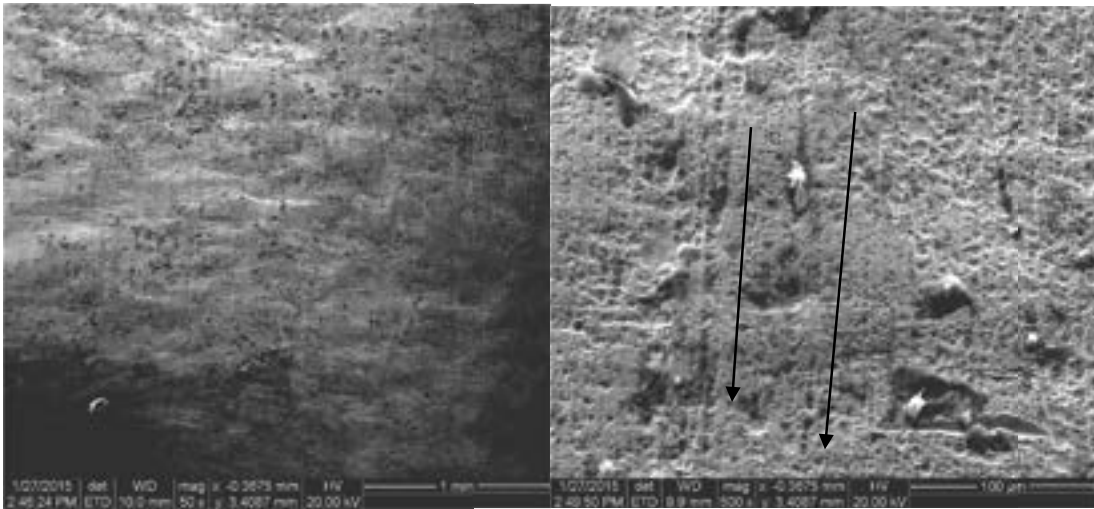


Figure 3-32. $\times 50$ and $\times 500$ magnification SEM images of 94UG top slice with curvature of U bend from top of image to bottom. Arrows denote machine tool directions.

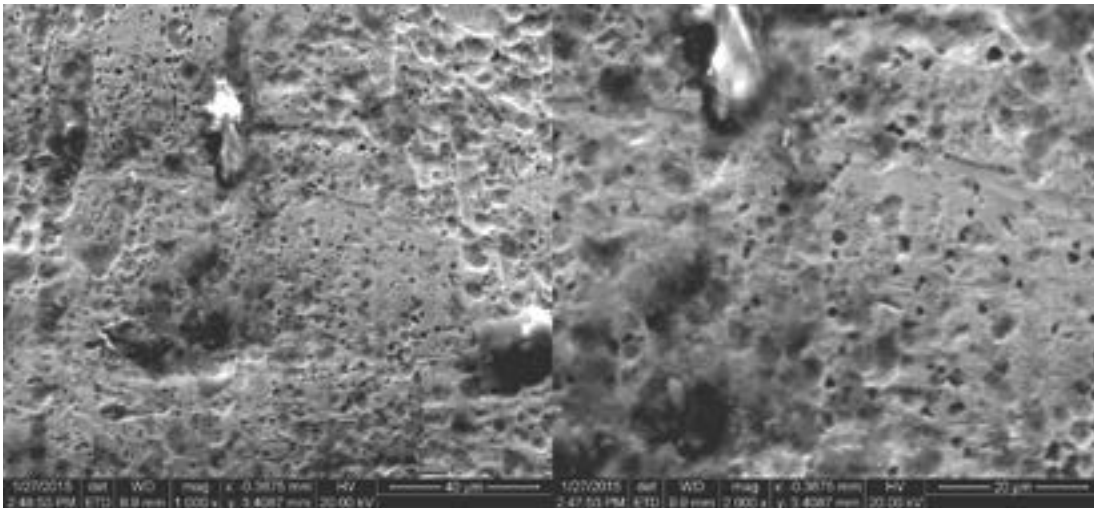


Figure 3-33. $\times 1000$ and $\times 2000$ magnification SEM images of 94UG top slice U bend with curvature from top of image to bottom.

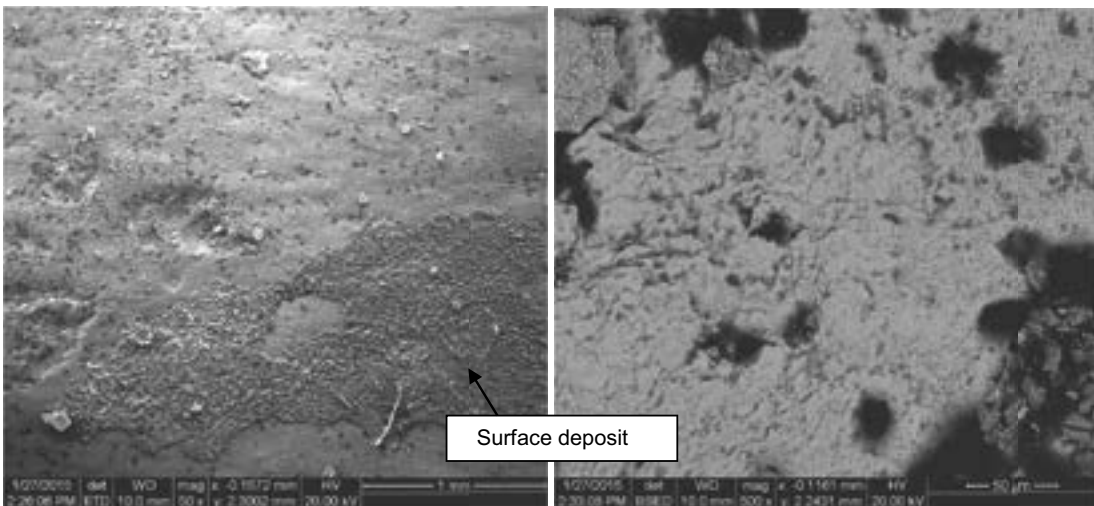
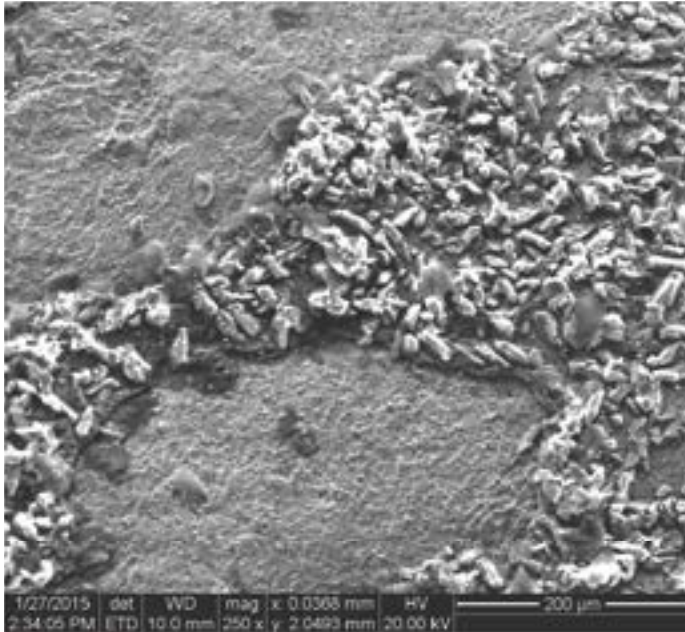


Figure 3-34. $\times 50$ and $\times 500$ magnification SEM images of 95UG unmounted slice with curvature of U bend from top of image to bottom.



| Element | |
|----------------|-----|
| Carbon | 49 |
| Oxygen | 14 |
| Iron | 7 |
| Calcium | 6 |
| Manganese | 0.1 |
| Copper | 18 |
| Other elements | 5.9 |

Figure 3-35. $\times 250$ magnification SEM image and elemental analysis (EDX) of surface deposit 95UG unmounted slice.

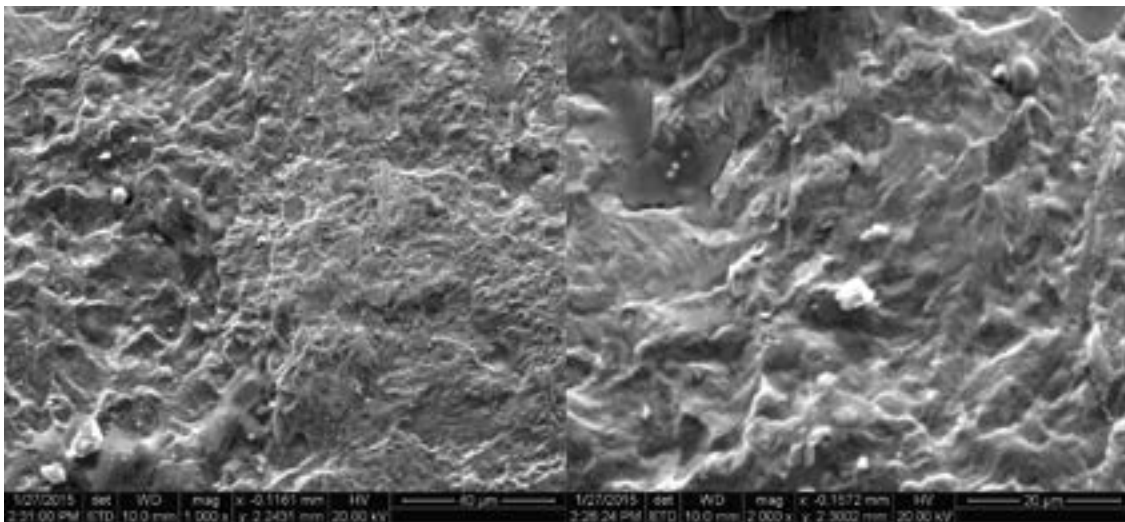


Figure 3-36. $\times 1000$ and $\times 2000$ magnification SEM images of 95UG unmounted slice U bend with curvature from top of image to bottom showing general surface corrosion.

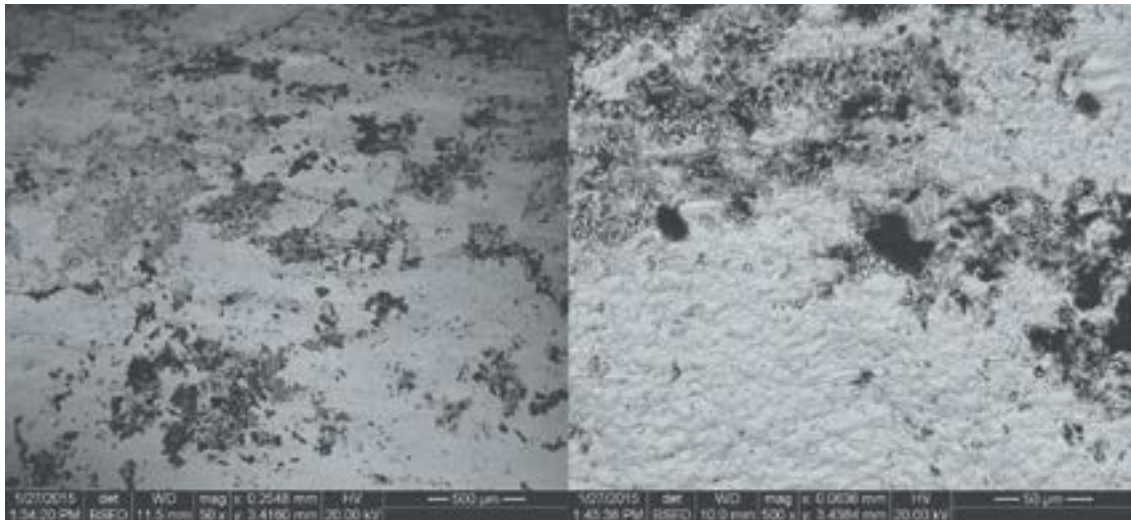


Figure 3-37. $\times 50$ and $\times 500$ magnification SEM images of 95UG top slice with curvature of U-bend from top of image to bottom.

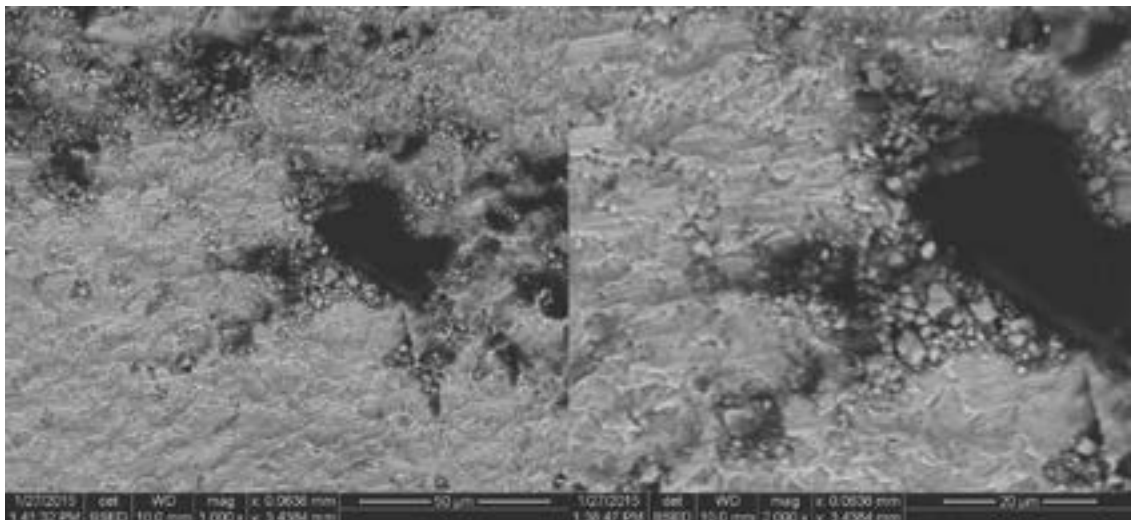


Figure 3-38. $\times 1000$ and $\times 2000$ magnification SEM images of 95UG top slice U bend with curvature from top of image to bottom.

Table 3-4. EDX weight percentage of elements (spot analysis – see Figure 3-29).

| Element | Position 1 | Position 2 | Position 3 |
|----------------|------------|------------|------------|
| Carbon | 34 | 39 | 39 |
| Oxygen | 38 | 14 | 9 |
| Molybdenum | 1 | 1 | 1.8 |
| Calcium | 23 | 2 | 0.4 |
| Copper | 4 | 41 | 49 |
| Other elements | – | 3 | 0.7 |

When compared with the untested U-bend, Specimen 94 UG shows evidence of pitting on the surface of the material. There appear to be striations of pits (i.e. selective attack), along the machine tool marks, as well as generally dispersed pits not associated with any machine tool marks. No significant difference in the EDX analysis of the pits was noted between the two types of corrosion (i.e. general corrosion and selective corrosion).

When comparing the surface condition of specimen 95UG with the untested U-bend, there was no evidence of pitting on the surface of the U-bend 95UG. This suggests that either the position of the U-bend in the MiniCan experiment is a variable to consider (unlikely) or that there had been general surface corrosion of one of the U-bends (94UG) when in storage after test and not for the other (95UG). A photograph of specimen 94UG immediately after it was removed from the experiment (Figure 3-39) does not show the presence of any significant corrosion, suggesting that corrosion occurred after the test during the storage period, when the specimens were stored in groundwater from Äspö. Although the containers were sealed in plastic boxes under inert gas and sealed in a secondary plastic bag, the possibility of oxygen ingress during storage over a period of approximately 18 months before they were analysed cannot be excluded (a green tint to the specimens was noted when the specimens were stored in groundwater, suggesting the possible formation of copper carbonate, malachite). XPS analysis of the surface of one leg of this specimen (Smart et al. 2012) showed that the surface film was predominantly composed of copper, oxygen and carbon, with a trace of sulphur.

95UG appears to have a considerable carbon- and oxygen-rich deposit on the surface of the material. This is shown in Figure 3-35, along with EDX data in the neighbouring table. This data further supports the possibility of calcium-copper carbonate being present on the surface of the tested U-bend specimens.



Figure 3-39. U-bend specimen 94UG immediately after removal from the water-filled transfer flask when the specimens were transported to the UK for analysis (Smart et al. 2012).

4 Overall Conclusions

The first task was to ascertain whether any crack growth that could be attributed to SCC had occurred from the pre-crack in the WOL specimens. The result of the investigation shows no evidence of any crack growth that can be attributed to SCC past the pre-crack area on the WOL fracture faces. However there was an oxygen-rich deposit coating the pre-crack area. The deposit on WOL A appeared to be thinner or less dense than the deposit on WOL B, which allowed the pre-crack region of WOL A to be imaged with greater detail. It is debatable whether any attempt to remove the deposit to analyse the fracture face morphology would be of benefit. Further investigation of the chemical composition of the deposit before removal is attempted would be useful so that a suitable cleaning procedure could be developed.

The second task of the investigation was to characterise the surface condition of the U-bends and to establish whether any pitting had occurred on the U-bend specimens in either the unstressed or stressed regions of the samples. This metallographic investigation has observed a range of features on the material surface. One U-bend specimen, 94UG, shows possible evidence of increased roughness along machining marks as well as general corrosion across the apex of the U-bend, but no increase in roughness / pitting on the flat parts of the U-bend specimen. The other U-bend (95UG) does not show definitive pitting but there is some limited evidence of general corrosion over the surface.

There was also evidence of a secondary surface finish effect caused by bending the copper strips into U-bends; this is known as an “orange peel” effect, which is due to non-uniform mechanical deformation of the grains in the copper alloy. The difference in strain across each grain depends on the direction of load applied with respect to each individual grain. This has resulted in non-uniform surface undulations across the apex of the U-bends. The mechanical deformation effect was confirmed by bending a third strip of copper (the untested copper strip) to the same bend angle under the same conditions as the tested U-bends.

Referring back to the previous report (Smart et al. 2013) and the question of whether or not pits were present in the cross-sections of the U-bends, it is likely that the specimen had been sliced through a particularly deep undulation rather than through a large pit. As described in the previous report (Smart et al. 2013), there is no evidence for extensive pitting having occurred. The morphology of the surface shown in Smart et al. 2013 (Figure 3-11, reproduced in Appendix A.3 of the current report) is probably due to the cross-section passing through non-uniform deformation that developed when the material was formed into a U-bend, as has been discussed previously (Smart et al. 2013, Rollason 1973, Chapter 7) and described in other literature (ASM 1994, Hatakeyama et al. 2002). If pitting had occurred it would be expected that there would have been more than one or two pits evident in the cross section.

There is also evidence of a C-Cu-Ca-O-rich deposit being present on the surface of the U-bends (possibly calcium-copper carbonate), which probably developed during post-test storage (in ground-water, in sealed containers that were probably not fully air tight). In future work, it would be beneficial to analyse any other test pieces within a shorter timeframe after they are removed for investigation.

References

SKB's (Svensk Kärnbränslehantering AB) publications can be found at www.skb.se/publications.

ASM, 1994. ASM handbook. Vol 5, Surface engineering. Materials Park, Ohio : ASM International.

Hatakeyama K, Sugawara A, Tojyo T, Ikeda K, 2002. Factors affecting bend formability of tempered copper alloy sheets. Materials Transactions 43, 2908–2912.

ISO 1302:2002. Geometrical Product Specifications (GPS) – Indication of surface texture in technical product documentation. Geneva: International Organization for Standardization.

ISO 4287:1997. Geometrical Product Specifications (GPS) – Surface texture: Profile method – Terms, definitions and surface texture parameters. Geneva: International Organization for Standardization.

Rollason E C, 1973. Metallurgy for engineers. 4th ed. London: Arnold.

Smart N, Rance A, Reddy B, Fennell P, Winsley R, 2012. Analysis of SKB MiniCan experiment 3. SKB TR-12-09, Svensk Kärnbränslehantering AB.

Smart N, Rose S, Nixon D, Rance A, 2013. Metallographic analysis of SKB MiniCan experiment 3. SKB R-13-35, Svensk Kärnbränslehantering AB.

A.1 Parameters for pre-cracking

Structural Integrity Services Department - Materials Testing Laboratory

| | | | |
|---|----------------|-------------|-----------|
| CT PRECRACKING CALCULATION SHEET | MTL | 6357 | Issue No. |
| | Job No. | | 9 |

SPREADSHEET NAME: **VERSION No.**

DESCRIPTION

Spreadsheet for calculating precracking loads. Specimen type: CT only. Room temp. pre-cracking only.
Calculation basis: From $K=(PY)/(BW^{0.5})$ using a/W at the end of the step

INSTRUCTIONS

Enter the data required in the **BOLD** outline boxes (pink on screen). Print out the table & sign.

SPECIMEN DETAILS

| | |
|---------------------------|------|
| Thickness, B, mm | 6.25 |
| Width, W, mm | 12 |
| Machined notch length, mm | 3.3 |

MATERIAL DETAILS

| | |
|-------------------------|-----|
| Yield/proof stress, MPa | 75 |
| Tensile strength, MPa | 150 |
| Elastic modulus, GPa | 117 |
| Estimated KIC, MPa√m | 50 |

CRACK REQUIREMENTS

| | |
|--------------------------|-----|
| Required a/W | 0.4 |
| Number of steps | 3 |
| Length of last step, mm* | 0 |

K REQUIREMENTS

| | |
|----------------|-----|
| Start K, MPa√m | 8.5 |
| End K, MPa√m | 8.5 |
| R ratio | 0.1 |

CALCULATED VALUES

| | | | |
|---------------------|-----|------------------------|-----|
| Length of crack, mm | 1.5 | Final crack length, mm | 4.8 |
|---------------------|-----|------------------------|-----|

LOAD TABLE

| Step No. | Crack length, mm | | P/c mm | a/W | K _{max} MPa√m | P _{max} kN | P _{min} kN | P _{mean} kN | ΔP ±kN | BFM** mm |
|----------|------------------|-------|-----------|-------|---------------------------|------------------------|------------------------|-------------------------|-----------|-------------|
| | Start | End | | | | | | | | |
| 1 | 3.300 | 3.800 | 0.500 | 0.317 | 8.5 | -0.99 | 0.10 | 0.55 | 0.45 | 8.200 |
| 2 | 3.800 | 4.300 | 1.000 | 0.358 | 8.5 | 0.89 | 0.09 | 0.49 | 0.40 | 7.700 |
| 3 | 4.300 | 4.800 | 1.500 | 0.400 | 8.5 | 0.80 | 0.08 | 0.44 | 0.36 | 7.200 |

* For steps of equal interval, enter a value of zero ** BFM = distance of scribe line from back face of specimen

VALIDITY See Tables on Page 2

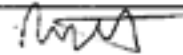
Number of validity failures reported is Number of warnings activated is

COMMENTS

| |
|--|
| |
|--|

SIGNED
(Test officer)

**CHECKED/
APPROVED**



A.2 Definition of surface roughness, R_a , where z is the surface height

$$R_a = \frac{1}{n} \sum_{i=1}^n |z_i|$$

A.3 Micrograph from Smart et al. (2013)

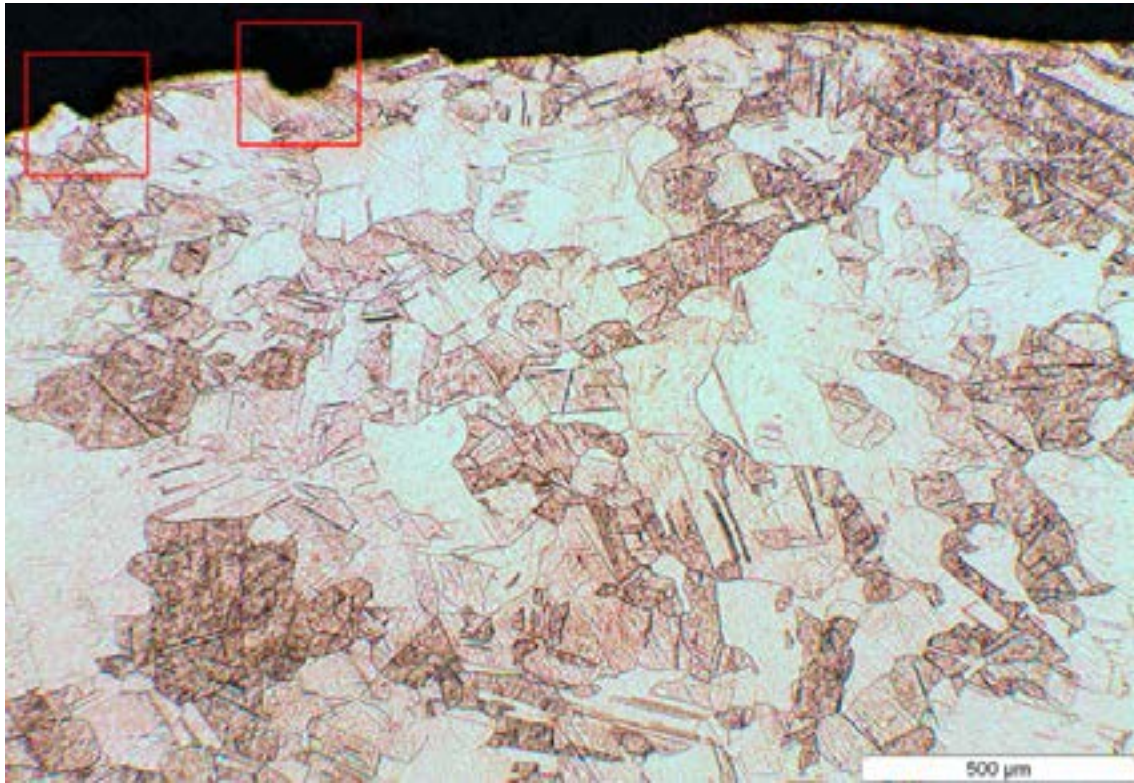


Figure A3-1. Optical micrograph of the outside cross-section of U-bend specimen 2 (near borehole flange), highlighting areas of surface roughness.

